Inorg. Chem. **2007**, *46*, 3336–3352

Influence of an Extremely Negatively Charged Porphyrin on the Reversible Binding Kinetics of NO to Fe(III) and the Subsequent Reductive Nitrosylation

Joo-Eun Jee,[†] Siegfried Eigler,[§] Norbert Jux,*[,§] Achim Zahl,[†] and Rudi van Eldik*[,†]

Institute for Inorganic Chemistry, University of Erlangen-Nürnberg, Egerlandstrasse 1, 91058 Erlangen, Germany, and Institute for Organic Chemistry, University of Erlangen-Nürnberg, Henkestrasse 42, 91054 Erlangen, Germany

Received September 13, 2006

The polyanionic, water-soluble, and non-μ-oxo dimer-forming iron porphyrin (hexadecasodium iron 5^4,10^4,15^4,20^4-tetra-*t*-butyl-5^2,5^6,10^2,10^6,15^2,15^6,20^2,20^6-octakis[2,2-bis(carboxylato)ethyl]-5,10,15,20-tetraphenylporphyrin), $(P^{16-})Fe^{III}$, with 16 negatively charged meso substituents on the porphyrin was synthesized and fully characterized by UV–vis and ^{1}H NMR spectroscopy. A single pK_{a1} value of 9.90 ± 0.01 was determined for the deprotonation of coordinated water in the six-coordinate $(P^{16-})Fe^{III}(H_2O)_2$ and as attributed to the formation of the five-coordinate monohydroxo-ligated form, $(P^{16-})Fe^{III}(OH)$. The porphyrin complex reversibly binds NO in aqueous solution to yield the nitric oxide adduct, $(P^{16-})Fe^{II}(NO^+)(L)$, where L = H_2O or OH^-. The kinetics for the reversible binding of NO were studied as a function of pH, temperature, and pressure using the stopped-flow technique. The data for the binding of NO to the diaqua complex are consistent with the operation of a dissociative mechanism on the basis of the significantly positive values of $\Delta S^{\ddagger}$ and $\Delta V^{\ddagger}$, whereas the monohydroxo complex favors an associatively activated mechanism as determined from the corresponding negative activation parameters. The rate constant, $k_{on} = 3.1 \times 10^4$ M^{-1} s^{-1} at 25 °C, determined for the NO binding to $(P^{16-})Fe^{III}(OH)$ at higher pH, is significantly lower than the corresponding value measured for $(P^{16-})Fe^{III}(H_2O)_2$ at lower pH, namely, $k_{on} = 11.3 \times 10^5$ M^{-1} s^{-1} at 25 °C. This decrease in the reactivity is analogous to that reported for other diaqua- and monohydroxo-ligated ferric porphyrin complexes, and is accounted for in terms of a mechanistic changeover observed for $(P^{16-})Fe^{III}(H_2O)_2$ and $(P^{16-})Fe^{III}(OH)$. The formed nitrosyl complex, $(P^{16-})Fe^{II}(NO^+)(H_2O)$, undergoes subsequent reductive nitrosylation to produce $(P^{16-})Fe^{II}(NO)$, which is catalyzed by nitrite produced during the reaction. Concentration-, pH-, temperature-, and pressure-dependent kinetic data are reported for this reaction. Data for the reversible binding of NO and the subsequent reductive nitrosylation reaction are discussed in reference to that available for other iron(III) porphyrins in terms of the influence of the porphyrin periphery.

Introduction

Nitric oxide (NO) is a versatile signaling molecule, and its interaction with metal-centered proteins plays an important role. In the human system, NO is associated with biological functions ranging from vasodilatation of vascular smooth muscle cells to neurotransmission, cytotoxic immune response, inflammation, and regulation of cell death.[1] It is generated in vivo by NO synthase in various organs from arginine with the aid of molecular oxygen and NADPH.[1,2] Nitric oxide is very reactive to Fe(II) and Fe(III), for which different electronic and structural factors of the iron center influence the chemical properties of the resulting nitrosyl

* To whom correspondence should be addressed. E-mail: vaneldik@chemie.uni-erlangen.de (R.v.E.); norbert.jux@organik.uni-erlangen.de (N.J.).
[†] Institute for Inorganic Chemistry.
[§] Institute for Organic Chemistry.

(1) (a) Moncada, S.; Higgs, E. A. *Br. J. Pharmacol.* **2006**, *147*, S104. (b) Valsova, I. I.; Tyurin, V. A.; Kapralov, A. A.; Kurnikov, I. V.; Osipov, A. N.; Potapovich, M. V.; Stoyanovsky, D. A.; Kagan, V. E. *J. Biol. Chem.* **2006**, *281*, 14554. (c) Feelisch, M.; Stamler, J. S. *Methods in Nitric Oxide Research*; John Wiley and Sons: Chichester, U.K., 1996. (d) Verma, A.; Hirsch, D. J.; Glatt, C. E.; Romnett, G. V.; Snyder, S. H. *Science* **1993**, *259*, 381. (e) Ribeiro, J. M. C.; Hazzard, J. M. H.; Nussenzveig, R. H.; Champagne, D. E.; Walker, F. A. *Science.* **1993**, *260*, 539. (f) Moncada, S.; Palmer, R. M. J.; Higgs, E. A. *Pharmacol. Rev.* **1991**, *43*, 109. (g) Moncada, S.; Radomski, L. W.; Palmer, R. M. *Biochem. Pharmacol*. **1988**, *37*, 2495. (h) Palmer, R. M. J.; Ferrige, A. G.; Moncada, S. *Nature.* **1987**, *327*, 524.

10.1021/ic061732g CCC: $37.00
Published on Web 03/22/2007

product, as well as the NO binding and dissociation rate constants. The reactivity of iron porphyrins is finely regulated by a variety of structural and electronic features, for example, the nature of the axial ligands, the type of substituents on the porphyrin periphery, the polarity of the reaction medium, and other factors. To investigate the role of these factors, numerous spectroscopic, structural, and mechanistic studies are reported on the interaction of NO with synthetic model complexes.[3]

Mechanistic studies on the reactions of NO with heme proteins or model ferric porphyrins have been performed by the application of laser flash photolysis and stopped-flow techniques. Studies on the reversible binding of NO to synthetic iron(II) and iron(III) porphyrins[4,5] and iron(III) heme proteins,[6a,7−10] such as cytochrome P450 and metmyoglobin, have been performed in which distinctive features of the active site of heme proteins were used to develop useful biomimetic model systems.

The binding of NO to an oxidizing metal (M^{n+}) induces intramolecular electron transfer, leading to the formation of $(P)M^{(n-1)+}-NO^+$, followed by nitrosylation of a nucleophile (Nu^-) to produce $(P)M^{(n-1)+}$ and Nu^--NO^+. The observed reaction involves reductive nitrosylation as expressed in reaction 1. Recent reports have supported that reductive nitrosylation is proposed as a viable pathway in which hemoglobin binds NO to the cys β-93 residue and forms *S*-nitrosohemoglobin in the transport and metabolism of NO.[11,12]

$$(P)M^{n+} + NO \overset{K_{NO}}{\rightleftharpoons} (P)M^{(n-1)+}-NO^+ \xrightarrow{+Nu^-} (P)M^{(n-1)+} + Nu^--NO^+ \quad (1)$$

On the basis of spectroscopic and kinetic data, the NO reduction of ferric-heme proteins (viz., ferric cytochrome c, metmyoglobin, and methemoglobin)[13−15] and synthetic model ferric porphyrins such as TPPS (tetra-(4-sulfonatophenyl)-porphyrinato), TMPyP (meso-tetrakis(*N*-methyl-4-pyridyl) porphyrinato),[6,16,17] P^{8+} (5,10,15,20-tetrakis-(4′-*t*-butyl-2′,6′-bis(4-*t*-butylpyridine)phenyl)-porphyrinato),[18] and P^{8-} (5^4,10^4,15^4,20^4-tetra-*t*-butyl-5^2,5^6,15^2,15^6-tetrakis-(2,2-bis-carboxylato-ethyl)-5,10,15,20-tetraphenylporphyrinato)[18] were systematically studied in aqueous medium, in which the resulting nitrosyl adducts ($(P)Fe^{III} + NO \rightarrow (P)Fe^{II}-NO^+$) interact with a nucleophile, namely, OH^- and NO_2^-, to yield ferroheme proteins. Recent studies performed in our laboratories clearly revealed that the observed rate constant for NO reduction depends on the concentration of NO and OH^- and suggested that the porphyrin environment involving oppositely charged substituents has a crucial influence on the observed rate constants and mechanistic features of nitrite-catalyzed reductive nitrosylation.[18]

The goal of these investigations is to understand the influence of the iron porphyrin microenvironment on the reactivity with NO and the stability of the resulting $(P)Fe^{II}-(NO^+)$ species toward subsequent reaction in aqueous solution. In this context, the reported studies were undertaken to investigate the systematic influence of the porphyrin environment on the properties and reactivity of water-soluble ferric porphyrins.[3−7] We now report the synthesis and spectroscopic characterization of an extremely negatively charged iron(III) porphyrin, $(P^{16-})Fe^{III}(L)_2$ (hexadecasodium iron 5^4,10^4,15^4,20^4-tetra-*t*-butyl-5^2,5^6,10^2,10^6,15^2,15^6,20^2,20^6-octakis[2,2-bis(carboxylato)ethyl)]-5,10,15,20-tetraphenylporphyrin) (Figure 1), and evaluate the detailed kinetics of its interaction with NO. In the latter context, variable pH-, temperature-, and pressure-dependent stopped-flow measurements provided a detailed kinetic and mechanistic description of the reversible binding of NO to $(P^{16-})Fe^{III}(H_2O)_2$ and $(P^{16-})Fe^{III}(OH)$ present in aqueous solution at low and high

(2) (a) Bredt, D. S.; Hwang, P. M.; Glatt, C. E.; Lowenstein, C.; Reed, R. R.; Snyder, S. H. *Nature (London)* **1991**, *351*, 714. (b) Steven, P. S.; Lewis, C. B.; David, A. K.; Hunter, C. C.; Michael, L. T.; Sandra, F.; Kavita, V. E.; Mark, D. K.; Susan, N. T.; Anne, C.; Joshua, H.; Gary, G. *J. Am. Med. Assoc.* **2006**, *295*, 58. (c) Moncada, S.; Palmer, R. M.; Higgs, E. A. *Biochem. Pharmacol.* **1989**, *38*, 1709. (d) Hibbs, J. B., Jr.; Tainter, R. R.; Vabrin, Z. *Science.* **1987**, *235*, 473.

(3) (a) Ford, P. C.; Laverman, L. E.; Lorkovic, I. M. *Adv. Inorg. Chem.* **2003**, *54*, 2003. (b) Ford, P. C.; Lorkovic, I. M. *Chem. Rev.* **2002**, *102*, 993, and references therein. (c) Hoshino, M.; Laverman, L. E.; Ford, P. C. *Coord. Chem. Rev.* **1999**, *187*, 75. (d) Laverman, L. E.; Ford, P. C. *J. Am. Chem. Soc.* **2001**, *123*, 11614. (e) Ford, P. C.; Fernandez, B. O.; Lim, M. D. *Chem. Rev.* **2005**, *105*, 2439. (f) Meunier, B. *Chem. Rev.* **1992**, *92*, 1411.

(4) (a) Wolak, M.; van Eldik, R. *J. Am. Chem. Soc.* **2005**, *127*, 13312 and references cited therein.

(5) (a) Jee, J.-E.; Eigler, S.; Hampel, F.; Jux, N.; Wolak, M.; Zahl, A.; Stochel, G.; van Eldik, R. *Inorg. Chem.* **2005**, *44*, 7717. (b) Jee, J.-E.; Wolak, M.; Balbinot, D.; Jux, N.; Zahl, A.; van Eldik, R. *Inorg. Chem.* **2006**, *45*, 1326 and references cited therein.

(6) (a) Theodoridis, A.; van Eldik, R. *J. Mol. Catal. A.* **2004**, *24*, 197. (b) Trofimova, N. S.; Safronov, A. Y.; Ikeda, S. *Inorg. Chem.* **2003**, *42*, 1945. (c) Hoshino, M.; Maeda, M.; Konishi, R.; Seki, H.; Ford, P. C. *J. Am. Chem. Soc.* **1996**, *118*, 5702.

(7) (a) Franke, A.; Stochel, G.; Suzuki, N.; Higuchi, T.; Okuzono, K.; van Eldik, R. *J. Am. Chem. Soc.* **2005**, *127*, 5360. (b) Wolak, M.; van Eldik, R. *Coord. Chem. Rev.* **2003**, *230*, 263. (c) Schneppensieper, T.; Zahl, A.; van Eldik, R. *Angew. Chem., Int. Ed.* **2001**, *40*, 1678.

(8) (a) Wyllie, G. R. A.; Scheidt, W. R. *Chem. Rev.* **2002**, *102*, 1067. (b) Ellison, M. K.; Schulz, Chapter E.; Scheidt, R. W. *J. Am. Chem. Soc.* **2002**, *124*, 13833.

(9) (a) Frank, A.; Jung, C.; van Eldik, R. *J. Am. Chem. Soc.* **2004**, *126*, 4181. (b) Suzuki, N.; Higuchi, T.; Urano, Y.; Kikuhchi, K.; Uchida, T.; Mukai, M.; Kitagawa, T.; Nagano, T. *J. Am. Chem. Soc.* **2000**, *122*, 12059. (c) Rich, A. M.; Armstrong, R. S.; Ellis, P. J.; Lay, P. A. *J. Am. Chem. Soc.* **1998**, *120*, 10827.

(10) Newman, K. E.; Meyer, F. K.; Merbach, A. E. *J. Am. Chem. Soc.* **1979**, *101*, 1470.

(11) Gladwin, M. T.; Ognibene, F. P.; Pannell, L. K.; Nochols, J. S.; Pease-Fye, M. E.; Shelhamer, J. H.; Schechter, A. N. *Free Radical Res.* **2000**, *97*, 9943.

(12) (a) Weichsel, A.; Maes, E. M.; Andersen, J. F.; Valenzuela, J. G.; Shokhireva, T. K.; Walker, F. A.; Montfort, W. R. *Proc. Natl. Acad. Sci. U.S.A.* **2005**, *102*, 594. (b) Gladwin, M. T.; Lancaster, J. R., Jr.; Freeman, B. A.; Schechter, A. N. *Nat. Med.* **2003**, *9*, 496. (c) Luchsinger, B. P.; Rich, E. N.; Gow, A. J.; Williams, E. M.; Stamler, J. S.; Singel, D. J. *Proc. Natl. Acad. Sci. U.S.A.* **2003**, *100*, 461. (e) Stamler, J. S.; Jia, L.; Eu, J. P.; Mcmahon, T. J.; Demchenko, I. T.; Bonaventura, J.; Gernert, K.; Piantadosi, C. A. *Science* **1997**, *276*, 2034. (f) Stamler, J. S.; Simon, D. I.; Osborne, J. A.; Mullins, M. E.; Jaraki, O.; Michel, T.; Singel, D. J.; Loscalzo, J. *Proc. Natl. Acad. Sci. U.S.A.* **1992**, *89*, 444. (g) Tran, D.; Skelton, B. W.; White, A. H.; Lavermann, L. E.; Ford, P. C. *Inorg. Chem.* **1998**, *37*, 2505.

(13) Yoshimura, T.; Suzuki, S.; Nakahara, A.; Iwasaki, H.; Masuko, M.; Matsubara, T. *Biochim. Biophys. Acta.* **1985**, *831*, 267.

(14) (a) Gow, A. J.; Luchsinger, B. P.; Pawloski, J. R.; Singel, D. J.; Stamler, J. S. *Proc. Natl. Acad. Sci. U.S.A.* **1999**, *96*, 9027. (b) Chien, J. C. W. *J. Am. Chem. Soc.* **1969**, *91*, 2166.

(15) Yoshimura, T.; Suzuki, S. *Inorg. Chim. Acta.* **1988**, *152*, 241.

(16) Tran, D.; Skelton, B. W.; White, A. H.; Lavermann, L. E.; Ford, P. C. *Inorg. Chem.* **1998**, *37*, 2505.

(17) Fernandez, B. O.; Lorkobic, I. M.; Ford, P. C. *Inorg. Chem.* **2004**, *43*, 5393.

(18) Jee, J.-E.; van Eldik, R. *Inorg. Chem.* **2006**, *45*, 6523.

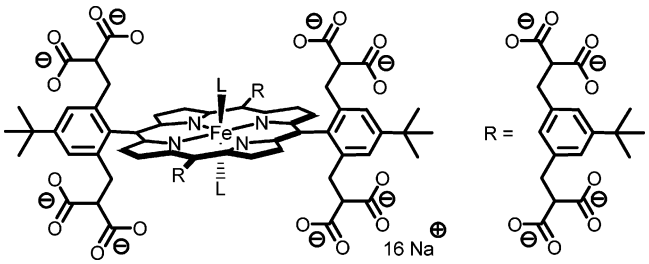

Figure 1. Structure of $(P^{16-})Fe^{III}(L)_2$ where L = H_2O or OH^-.

pH, respectively. The subsequent reductive nitrosylation was also studied as a function of concentration, temperature, and pressure. The results are discussed in reference to kinetic data and mechanistic information reported for other water-soluble iron(III) porphyrins.

Experimental Section

Synthesis and Characterization of $(P^{16-})Fe^{III}$. The chemicals and solvents employed for the synthesis of $(P^{16-})Fe^{III}$ were used as received unless otherwise noted. Solvents were dried using standard procedures. Column chromatography was performed on silica gel 60, 32−63 μm, 60 Å (MP Biomedicals). Standard ^{1}H and ^{13}C NMR spectra were recorded on a Bruker Avance 300 spectrometer. FAB mass spectrometry was performed with Micromass Zabspec. Standard UV−vis spectra were recorded on a Shimadzu UV-3102 PC UV−vis NIR scanning spectrophotometer. IR spectra (KBr pellets) were recorded with a FT-IR IFS 88 infrared spectrometer (Bruker Analytische Messtechnik GmbH). Elemental analyses were carried out on a CHN-Mikroautomat (Heraeus). Thin-layer chromatography (TLC) was carried out on E. Merck silica gel 60 F254 plates. Zinc(II)-5^4,10^4,15^4,20^4-tetra-*t*-butyl-5^2,5^6,10^2,-10^6,15^2,15^6,20^2,20^6-octabromo-5,10,15,20-tetraphenylporphyrin (**2**) was synthesized as described previously.[19]

Zinc(II)-5^4,10^4,15^4,20^4-tetra-*t*-butyl-5^2,5^6,10^2,10^6,15^2,15^6,20^2,20^6-octakis[2,2-bis(methoxycarbonyl)ethyl)]-5,10,15,20-tetraphenylporphyrin (3). KH (24 mg, 0.60 mmol) was suspended in DMF (20 mL) under a N_2 atmosphere. Dimethyl malonate (160 mg, 1.20 mmol in 20 mL DMF) was added dropwise at room temperature (rt). After an additional hour, porphyrin **2** (100 mg, 0.061 mmol) was added, and the solution was stirred for 4 h at rt. The reaction mixture was poured onto an ice/water mixture to precipitate the product. The solid was filtered and washed thoroughly with water. The purple residue was dissolved in CH_2Cl_2, dried over $MgSO_4$, and concentrated in vacuum. The product was further purified by column chromatography (SiO_2, CH_2Cl_2/EtOAc 10:1) and was obtained as a purple solid. Yield: 104 mg (83%, 0.050 mmol). ^{1}H NMR (400 MHz, $CDCl_3$, rt): δ 8.64 (s, 8H, β-pyrr-*H*), 7.43 (s, 8H, *o*-Ar-*H*), 3.18 (s, 48H, C*H*$_3$), 3.07 (t, 8H,^3J = 8.3 Hz, C*H*), 2.79 (d, 16H,^3J = 8.3 Hz, Ar−C*H*$_2$), 1.52 (s, 36H, C*H*$_3$). ^{13}C NMR (75 MHz, $CDCl_3$, rt): δ 169.0, 151.2, 150.1, 139.3, 139.0, 131.4, 124.6, 115.7, 52.2, 51.9, 34.8, 34.1, 31.6. MS (FAB, NBA): *m*/*z* 2055 ($M^{+\cdot}$). IR (KBr): ν [cm^{-1}] 2957, 2907, 2872, 1737, 1436, 1332, 1285, 1227, 1200, 1150, 1065, 1027, 992, 883, 799, 725. UV−vis (CH_2Cl_2): λ [nm] (ϵ [mol^{-1} cm^{-1}]) 430 (3.94 × 10^5), 561 (1.27 × 10^4), 599 (1.1 × 10^3).

5^4,10^4,15^4,20^4-Tetra-*t*-butyl-5^2,5^6,10^2,10^6,15^2,15^6,20^2,20^6-octakis-[2,2-bis(methoxycarbonyl)ethyl)]-5,10,15,20-tetraphenylporphyrin (4). HCl (6 M, 50 mL) was added to a solution of **3** (80 mg, 0.039 mmol) in CH_2Cl_2 (50 mL), and the two layers were shaken vigorously. The green (organic) layer was shaken once again with 2 M HCl (50 mL) and twice with water (50 mL each). After neutralization with a saturated $NaHCO_3$ solution (50 mL) and a final wash with brine (50 mL), the organic layer was dried with $MgSO_4$, and the solvent was removed under reduced pressure. The compound was further cleaned by column chromatography (silica gel, CH_2Cl_2/ethyl acetate 9:1) and was obtained as a purple powder. Yield: 76 mg (98%, 0.038 mmol). ^{1}H NMR (300 MHz, $CDCl_3$, rt): δ 8.71 (s, 8H, β-pyrr-*H*), 7.45 (s, 8H, *o*-Ar-*H*), 3.16 (t, 8H,^3J = 8.2 Hz, C*H*), 3.12 (s, 48H, C*H*$_3$), 2.79 (d, 16H,^3J = 8.2 Hz, Ar−C*H*$_2$), 1.53 (s, 36H, C*H*$_3$), −2.51 (s, 2H, N*H*). ^{13}C NMR (75 MHz, $CDCl_3$, rt): δ 168.6, 151.7, 139.1, 137.8, 124.4, 115.7, 51.9, 51.8, 34.8, 33.7, 31.5. MS (FAB, NBA): *m*/*z* 1991 ($M^{+\cdot}$), 1932 ($M^{+\cdot}$ − $COOCH_3$). IR (KBr): ν [cm^{-1}] 2957, 2907, 2872, 1733, 1606, 1559, 1436, 1343, 1278, 1227, 1197, 1150, 1061, 1027, 965, 887, 868, 803, 737. UV−vis (CH_2Cl_2): λ [nm] (ϵ [mol^{-1} cm^{-1}]) 422 (4.31 × 10^5), 517 (1.67 × 10^4), 550 (2.3 × 10^3), 593 (3.7 × 10^3), 646 (1.0 × 10^3).

Chloroiron(III) 5^4,10^4,15^4,20^4-Tetra-*t*-butyl-5^2,5^6,10^2,10^6,15^2,-15^6,20^2,20^6-octakis[2,2-bis(methoxycarbonyl)ethyl)]-5,10,15,20−5,10,15,20-tetraphenylporphyrin (5). $FeCl_2$ (230 mg, 1.81 mmol) was added to a solution of **4** (230 mg, 0.12 mmol) in THF (30 mL), and the mixture was heated under reflux for 24 h. The solvent was evaporated, and the residue was dissolved in CH_2Cl_2 and washed with 6 M HCl. The organic layer was separated and washed twice with water. After it was dried over $MgSO_4$, the compound was precipitated to give a dark brown powder. Yield: 189 mg (73%, 0.088 mmol). ^{1}H NMR (300 MHz, $CDCl_3$, rt): δ 82.6 (br s, β-pyrr-*H*), 16.6, 14.6 (br s, aryl-*H*). MS (FAB, NBA): *m*/*z* 2046 (M^+ − Cl). IR (KBr): ν [cm^{-1}] 2957, 2907, 2872, 1733, 1606, 1436, 1227, 1197, 1150, 1031, 995, 883, 837, 802, 725. UV−vis (CH_2Cl_2): λ [nm] (ϵ [mol^{-1} cm^{-1}]) 391 (5.85 × 10^5), 427 (9.39 × 10^5), 517 (1.38 × 10^4), 579 (3.8 × 10^3), 692 (2.7 × 10^3).

Hexadecasodium Hydroxoiron(III) 5^4,10^4,15^4,20^4-Tetra-*t*-butyl-5^2,5^6,10^2,10^6,15^2,15^6,20^2,20^6-octakis[2,2-bis(carboxylato)ethyl)]-5,10,15,20-tetraphenylporphyrin (1-OH). NaOH (1.50 g, 37.5 mmol) was added to a solution of **5** (150 mg, 0.072 mmol) in ethanol (20 mL), and the reaction mixture was heated under reflux for 2 h. After the mixture was cooled to room temperature, the precipitate was filtered, washed with ethanol (200 mL), and dried under reduced pressure. Gel permeation chromatography (Sephadex LH20) in methanol and the subsequent precipitation with diethyl ether gave a dark brown powder which, according to the microanalysis, contains sodium hydroxide in the lattice. Yield: 230 mg (86%, 0.061 mmol, based on formula obtained by microanalysis). ^{1}H NMR (300 MHz, pD = 7, rt): δ 48.6 (br s, β-pyrr-*H*), 9.71, 3.75, 2.81. IR (KBr): ν [cm^{-1}] 2964, 2876, 1563, 1405, 1359, 1332, 1290, 1065, 999, 876, 837, 802. UV−vis (H_2O, unbuffered): λ [nm] (ϵ [mol^{-1} cm^{-1}]) 324 (2.4 × 10^4), 401 (7.5 × 10^4), 510 (1.0 × 10^4). Anal. Calcd for $C_{92}H_{77}FeN_4Na_{16}O_{33}$ 38NaOH: C, 29.78; H, 3.12; N, 1.51. Found: C, 29.48; H, 3.24; N, 1.27.

Materials. Mes, Bis-Tris, Taps, sodium borate, Caps, and NaOH were used as buffer solutions and were purchased from Sigma-Aldrich. All chemicals used in this study were of analytical grade reagent. The NO gas (Messer Griesheim or Riessner Gase, ≥99.5 vol %) was purified from impurities of nitrogen oxides such as NO_2 and N_2O_3 by being passed through an Ascarite II column (NaOH on silica gel from Sigma-Aldrich) and concentrated NaOH solution.

Solution Preparation. All solutions were prepared under strict oxygen-free conditions with Milli-Q water and handled in gastight glassware because of the high oxygen-sensitivity of NO and the nitrosyl complexes. Oxygen-free Ar and N_2 were used to prepare

(19) Jux, N. *Org. Lett.* **2000**, *2*, 2129.

deoxygenated solutions. Buffered solutions of the appropriate pH for stopped-flow measurements were prepared with Mes, Bis-Tris, Taps, sodium borate, and Caps buffers at a concentration of 0.05M. The pH of the solution was controlled with $HClO_4$ and NaOH. The ionic strength was kept constant at 0.1 M with $NaClO_4$.

Measurements. pH measurements were carried out on a Metrohm 623 pH meter equipped with a Sigma glass electrode. A NO electrode (World Precision Instruments isolated nitric oxide meter, model ISO-NO) was used to determine the concentration of NO gas in aqueous solution. The NO electrode was calibrated with a freshly prepared KNO_2 solution according to the method suggested by the manufacturer. UV−vis spectra were recorded in gastight cuvettes on a Shimadzu UV−2100 spectrophotometer equipped with a thermostated cell compartment CDS-260. UV−vis spectra at pressures up to 150 MPa were recorded in a custom-built high-pressure optical cell.[20]

Stopped-flow kinetic measurements on the reaction of NO with $(P^{16-})Fe^{III}$ at pH 6.5 and 12.7 were carried out with an Applied Photophysics SX−18MV stopped-flow spectrophotometer. Deoxygenated aqueous solutions of $(P^{16-})Fe^{III}$ were rapidly mixed in varying volume ratios with a saturated NO solution in a gastight syringe to obtain the appropriate NO concentration (0.2−2 mM). The kinetics of the reaction were monitored at 430 and 435 nm where the change in absorbance is a maximum for the nitrosyl adducts at pH 6.5 and 12.7, respectively. The rates of NO binding (k_{on}) and release (k_{off}) were determined from the slope and intercept of linear plots of k_{obs} versus [NO], respectively, as described in more detail in the Results and Discussion. More accurate NO dissociation rates at different temperatures and pressures were measured directly by the NO-trapping method, in which $[Ru^{III}(edta)(H_2O)]^-$ was used as an efficient NO scavenger. This involved rapid mixing of a $(P^{16-})Fe^{II}(NO^+)(L)$, L = H_2O or OH^-, solution (2×10^{-5} M, L = H_2O and OH^- at pH 6.5 and 12.7, respectively) containing a small excess of NO with aqueous solutions of $[Ru^{III}(edta)(H_2O)]^-$ (1−2 mM) to give $[Ru^{III}(edta)(NO)]^-$ and $(P^{16-})Fe^{III}(L)_2$, as shown by the observed spectral change. The kinetics of NO release was followed in the stopped-flow spectrophotometer at 430 (pH 6.5) or 435 nm (pH 12.7). We also measured the rate constants for the conversion of $(P^{16-})Fe^{II}(H_2O)(NO^+)$ to $(P^{16-})Fe^{II}(NO)$. The observed rate constants and activation parameters for the reactions with NO/nitrite were monitored at 431 nm where the change in absorbance is at a maximum. All kinetic experiments were performed under pseudo-first-order conditions, that is, with at least a 10-fold excess of NO over the iron porphyrin. Reported rate constants are the mean values of at least five kinetics runs, and the quoted uncertainties are based on the standard deviation. High-pressure stopped-flow studies were performed on a custom-built instrument (from 10 to 130 MPa).[21] Kinetic traces were recorded on an IBM-compatible computer and analyzed with the OLIS KINFIT (Bogart, GA) set of programs.

^{17}O NMR Water Exchange Measurements. Rate constants for water exchange on the paramagnetic $(P^{16-})Fe^{III}$ complex and the corresponding activation parameters, $\Delta H^{\ddagger}_{ex}$, $\Delta S^{\ddagger}_{ex}$, and $\Delta V^{\ddagger}_{ex}$, were measured at pH 6.5 and 12.7 using a ^{17}O NMR line-broadening technique. Aqueous solutions of $(P^{16-})Fe^{III}$ (20 mM) were prepared at pH 6.5 (Mes buffer solution adjusted with $HClO_4$) and 12.7 (with NaOH). Both solutions were kept at 0.1 M $NaClO_4$ for the approximate ionic strength, in which 10% of the total sample volume of enriched ^{17}O-labeled water (normalized 19.2% ^{17}O H_2O, D-Chem Ltd) was added to each solution. A sample containing the same components without the $(P^{16-})Fe^{III}$ complex was used as a reference. Variable-temperature and -pressure Fourier transform ^{17}O NMR spectra were recorded at a frequency of 54.24 MHz on a Bruker Advance DRX 400WB spectrometer. The temperature dependence of the $^{17}OH_2$ line broadening was studied in the range of 278−353 K. A homemade high-pressure probe[22] was used for the variable-pressure experiments performed at the selected temperature (at 293 K at pH 6.5) and in the pressure range of 1−150 MPa. The sample was placed in a standard 5 mm NMR tube cut to a length of 45 mm. Hydrostatic pressure was transmitted to the sample by a movable macor piston, and the temperature was controlled as described elsewhere.[22] The reduced transverse relaxation times ($1/T_{2r}$) were calculated for each temperature and pressure from the difference in the line widths observed in the presence and absence of the metal complex, ($\Delta\nu_{obs} - \Delta\nu_{solvent}$). The reduced transverse relaxation time is related to the exchange rate constant $k_{ex} = 1/\tau_m$ (where τ_m is the mean coordinated solvent lifetime) and to the NMR parameters by the Swift and Connick equation (2a),[22,23]

$$\frac{1}{T_{2r}} = \pi \frac{1}{P_m}(\Delta\upsilon_{obs} - \Delta\upsilon_{solvent}) = \frac{1}{\tau_m}\left\{\frac{T_{2m}^{-2} + (T_{2m}\,\tau_m)^{-1} + \Delta\omega^2_m}{(T_{2m}^{-1} + \tau_m^{-1})^2 + \Delta\omega^2_m}\right\} + \frac{1}{T_{2os}} \quad (2a)$$

where P_m is the mole fraction of water coordinated to the Fe(III) ion, T_{2os} represents the outer-sphere contribution to T_{2r} arising from long-range interactions of unpaired electrons of Fe(III) with the water outside the coordination sphere, T_{2m} is the transverse relaxation time of water in the inner coordination sphere in the absence of chemical exchange, and $\Delta\omega_m$ is the difference in the resonance frequency of ^{17}O nuclei in the first coordination sphere of the metal and in the bulk solvent. In the present system, the contribution of $1/T_{2os}$ to $1/T_{2r}$ and $1/T_{2m}$ is negligible, so that eq 2a can be reduced to eq 2b. Taking into account that the temperature

$$\frac{1}{T_{2r}} = \pi \frac{1}{P_m}(\Delta\upsilon_{obs} - \Delta\upsilon_{solvent}) = \frac{1}{\tau_m}\left\{\frac{T_{2m}^{-2} + (T_{2m}\tau_m)^{-1} + \Delta\omega^2_m}{(T_{2m}^{-1} + \tau_m^{-1})^2 + \Delta\omega^2_m}\right\} \quad (2b)$$

dependence of k_{ex} is given by eq 2c (taken from transition state theory), the NMR and kinetic parameters were calculated by the use of a nonlinear least-squares method applied to eq 2b in which $1/\tau_m$ was replaced by eq 2c.

$$k_{ex} = \frac{1}{\tau_m} = (k_B T/h)\exp\{(\Delta S^{\ddagger}_{ex}/R) - (\Delta H^{\ddagger}_{ex}/RT)\} \quad (2c)$$

The temperature dependence of $\Delta\omega_m$ was assumed to be a simple reciprocal function A/T,[8,24] where A was determined as a parameter in the treatment of the line-broadening data. The exchange rate constant is assumed to have a simple pressure dependence given by eq 2d where k_{ex}^0 is the rate constant for solvent exchange at

$$k_{ex} = \frac{1}{\tau_m} = k_{ex}^0 \exp\{(-\Delta V^{\ddagger}_{ex}/RT)P\} \quad (2d)$$

atmospheric pressure. The pressure-dependent measurements were performed at a temperature close to the optimal exchange region (i.e., around the maximum of the plot of $\ln(1/T_{2r})$ versus $1/T$). The

(20) Spitzer, M.; Gartig, F.; van Eldik, R. *Rev. Sci. Instrum.* **1988**, *59*, 2092.
(21) van Eldik, R.; Gaede, W.; Wieland, S.; Kraft, J.; Spitzer, M.; Palmer, D. A. *Rev. Sci. Instrum.* **1993**, *64*, 1355.
(22) Zahl, A.; Neubrand, A.; Aygen, S.; van Eldik, R. *Rev. Sci. Instrum.* **1994**, *65*, 882.

Scheme 1. Synthesis of $(P^{16-})Fe^{III}$

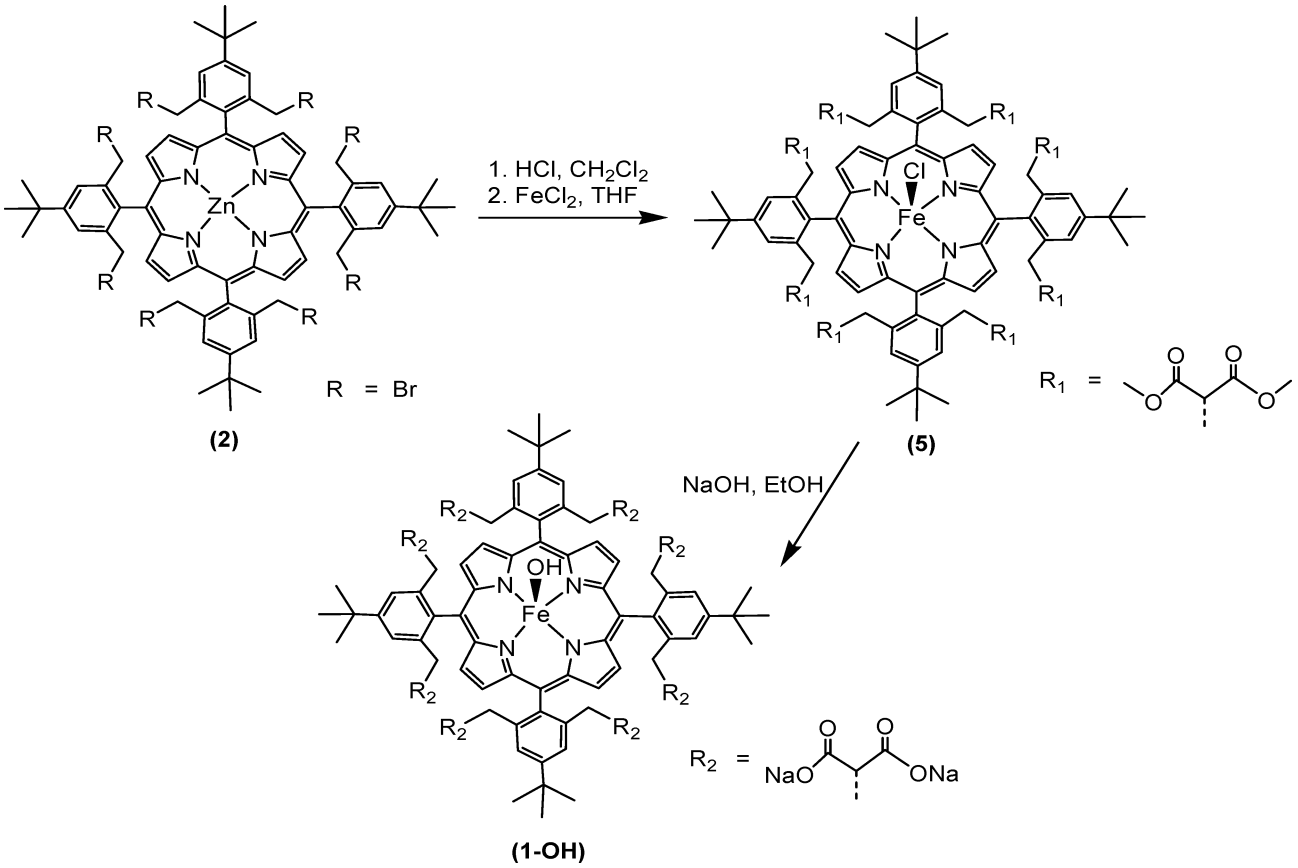

reduced relaxation time, T_{2r}, and the value of $\Delta\omega_m$ (calculated using the value of A determined from the temperature dependence and assumed to be pressure independent) were substituted into eq 2b to determine k_{ex} at each pressure. The resulting plot of $\ln(k_{ex})$ versus pressure was linear, and the volume of activation was calculated directly from the slope ($-\Delta V^{\ddagger}_{ex}/RT$). The value of k_{ex}^0 obtained from the plot of $\ln(k_{ex})$ versus P by extrapolation to atmospheric pressure was in good agreement with the corresponding value for k_{ex} from the temperature-dependent measurements at ambient pressure. In analogous temperature-dependent ^{17}O NMR measurements performed for the $(P^{16-})Fe^{III}$ complex at pH 12.7 (0.05M NaOH), the line-width differences in the presence and absence of the metal complex were very small, indicating the absence of a significant water-exchange process for the $(P^{16-})Fe^{III}$ form present at higher pH. Because of the small observed differences, the data obtained in the variable-temperature study did not enable a reliable fit to the Swift and Connick equation.

Electrochemical Measurement. Cyclic voltammetry measurements were carried out using an Autolab PGSTAT 30 system (Eco Chemie). A conventional three-electrode arrangement was employed consisting of a gold disk working electrode (geometric area = 0.07 cm^2), a platinum wire auxiliary electrode, and a Ag/AgCl, NaCl (3 M) reference electrode, manufactured by Metrohm. The measurements in aqueous solution were performed in 0.1 M Bis-tris electrolyte and 25 °C. The complex concentration was 1 mM. The solution was initially thoroughly degassed with purified nitrogen (15 min), and a stream of N_2 gas was passed over the sample solutions during the measurements.

Results and Discussion

Synthesis of $(P^{16-})Fe^{III}$ (1). We choose porphyrin **2** as a starting material[19] because its bromomethyl groups can be substituted easily with potassium malonates to yield the malonate ester porphyrin **3**. Demetalation with concentrated hydrochloric acid transformed **3** into the free-base porphyrin **4** as shown in Scheme 1. Subsequent reaction with ferrous chloride in THF gave the neutral iron(III) porphyrin octamalonic ester system **5**. ^1H NMR and UV−vis spectroscopic data clearly show that **5** is a paramagnetic iron(III) porphyrin with a single chloro axial ligand. The β-pyrrole ^1H resonance at 82.6 ppm (half-width of ~300 Hz) indicates the overall C_{4v} symmetry of the porphyrin and proves the $S = 5/2$ spin state.[25] Saponification of the malonic esters of **5** with sodium hydroxide in ethanol leads to precipitation of a brownish material that is soluble in water but totally insoluble in apolar solvents. Gel permeation chromatography (Sephadex LH20) in methanol and subsequent precipitation with diethyl ether gave a solid material containing about 75% of **1** (the impurities being NaOH and H_2O) as was found earlier for **$(P^{8-})Fe^{III}$** in a similar way.[5a] Standard NMR spectra measured in unbuffered D_2O have shown that under these conditions **1** exists as a high-spin monohydroxo complex **$(P^{16-})Fe^{III}(OH)$** (β-pyrrole ^1H at 80.0 ppm, see also further text).

(23) Schneppensieper, T.; Seibig, S.; Zahl, A.; Tregloan, P.; van Eldik, R. *Inorg. Chem.* **2001**, *40*, 3670.
(24) (a) Swift, T. J.; Connick, R. E. *J. Chem. Phys.* **1962**, *37*, 307. (b) Swift, T. J.; Connick, R. E. *J. Chem. Phys.* **1964**, *41*, 2553.
(25) (a) Woon, T. C.; Shirazi, A.; Bruice, T. *Inorg. Chem.* **1986**, *25*, 3845. (b) Cheng, R.-J.; Latos-Grazynski, L.; Balch, A. *Inorg. Chem.* **1982**, *21*, 2412.

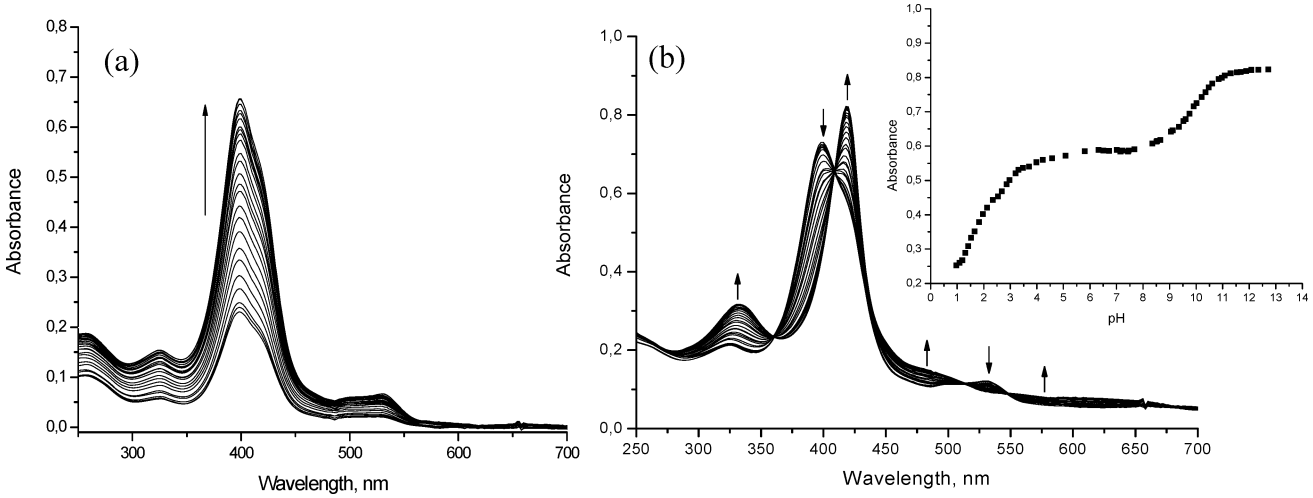

Figure 2. UV−vis spectral changes observed for aqueous solutions of $(P^{16-})Fe^{III}$ in the pH ranges of (a) 1−6 and (b) 6−13. The inset shows a plot of the absorbance at 420 nm versus the pH in the range of 1−13. Experimental conditions: $[(P^{16-})Fe^{III}] = 1.1 \times 10^{-4}$ M, temp = 25 °C, $I = 0.1$ M (with $NaClO_4$).

Two structural details which are important with regard to the investigations presented in this paper can be extracted from the previously shown crystal structure of the zinc precursor of $(P^{8-})Fe^{III}$ crystallized from THF.[5a] First, the malonate groups are located above and below the porphyrin plane, thus not allowing for the formation of μ-oxo-dimer formation for steric and electrostatic reasons (as confirmed by in-depth spectroscopic studies described below). Second, the malonate groups cannot coordinate to the metal center in an intramolecular fashion without extreme distortion of the molecule (the average distance of the malonate oxygen atoms from the zinc atom is ∼7 Å, and the closest distance is ∼4 Å). Nevertheless, ester or carboxylate groups of malonate substituents may interact with axial ligands coordinated to the metal center.

Studies on $(P^{16-})Fe^{III}$. The speciation of $(P^{16-})Fe^{III}$ as a function of pH in aqueous medium was studied by UV−vis, ^1H NMR, and ^{17}O NMR techniques. A spectrophotometric titration of a $(P^{16-})Fe^{III}$ solution in the pH range of 1−13 at 0.1 M ionic strength (adjusted with $NaClO_4$) resulted in the spectral changes presented in Figure 2. The spectral changes are separated into two parts, and the corresponding plot of absorbance at 420 nm versus pH is shown in the inset of Figure 2b. In the pH range of 1−6, the absorbance continuously increases over the whole spectral range as a result of the deprotonation of the carboxylic acid groups upon increasing the pH which is accompanied by an increase in the solubility of the porphyrin complex (see Figure 2a). As can be seen in Figure 2b, an increase in pH from 6 to 13 leads to a gradual shift of the peaks at 398 ($\epsilon = 6.4 \times 10^4$ M^{-1} cm^{-1}) and 532 nm ($\epsilon = 1.04 \times 10^4$ M^{-1} cm^{-1}) to 418 ($\epsilon = 7.2 \times 10^4$ M^{-1} cm^{-1}) and 606 nm ($\epsilon = 7.1 \times 10^3$ M^{-1} cm^{-1}). The observed pattern is similar to that reported for other water-soluble iron(III) porphyrins and typical for the formation of monohydroxo-ligated species from the corresponding diaqua-ligated $(P)Fe^{III}(H_2O)_2$.[25,26] No further spectral changes occurred in solution at high pH upon extended standing, and the observed spectral changes in the pH range of 6−13 were fully reversible. This indicates rapid interconversion of species present at high and low pH upon changing the pH and suggests that the possible formation of a μ-oxo dimer does not occur in the present system. This interpretation is further supported by the NMR data reported below. Two pK_a values were determined from the plot in Figure 2b, from which the first pK_a of ∼2 in the range of $1 < pH < 6$ is attributed to the deprotonation of the carboxylic acid groups (reaction 3) on the modified porphyrin in reference to the pK_a values for benzylmalonic acid of 2.56 and 5.22.[5] The second $pK_{a1} = 9.90 \pm 0.01$ in the pH range of 6−13 is attributed to the deprotonation of coordinated water as described by reaction 4.

$$(H_{16}P)Fe^{III}(H_2O)_2 \rightleftarrows (P^{16-})Fe^{III}(H_2O)_2 + 16\ H^+ \qquad 1 < pK_{a(RCOOH)} < 6 \quad (3)$$

$$(P^{16-})Fe^{III}(H_2O)_2 \rightleftarrows (P^{16-})Fe^{III}(H_2O)(OH^-) + H^+ \qquad pK_{a1} = 9.90 \pm 0.01 \quad (4)$$

On the basis of the data summarized in Table 1, the pK_{a1} value for $(P^{16-})Fe^{III}(H_2O)_2$ is the highest value reported for water-soluble iron(III) porphyrins so far and must be related to the extremely negative charge on the porphyrin substituents, which increases the electron density on the iron(III) center in $(P^{16-})Fe^{III}(H_2O)_2$ and, as a result, increases the pK_{a1} value. Another reason for the high pK_{a1} value can be related to the through-space interaction of deprotonated carboxylate groups of the flexible malonate substituents on the porphyrin with the coordinated water molecules stabilized by hydrogen bonding, as reported for other negatively charged water-soluble ferric porphyrins, namely, $(P^{8-})Fe^{III}(H_2O)_2$ and $(TanP^{4-})Fe^{III}(H_2O)_2$.[5a,27]

^1H NMR measurements were carried out for (P^{16-})-$Fe^{III}(H_2O)_2$ and $(P^{16-})Fe^{III}(H_2O)(OH^-)$ at pD values of 6.5

(26) (a) El-awady, A. A.; Wilkins, P. C.; Wilkins, R. G. *Inorg. Chem.* **1985**, *24*, 2053. (b) Miskelly, G. M.; Webley, W. S.; Clark, Ch. R.; Buckingham, D. A. *Inorg. Chem.* **1988**, *27*, 3773. (c) Kobayashi, N. *Inorg. Chem.* **1985**, *24*, 3324. (d) Tondreau, G. A.; Wilkins, R. G. *Inorg. Chem.* **1986**, *25*, 2745. (e) Zipplies, M. F.; Lee, W. A.; Bruice, T. C. *J. Am. Chem. Soc.* **1986**, *108*, 4433.

(27) Imai, H.; Yamashita, Y.; Nakagawa, S.; Munakata, H.; Uemori, Y. *Inorg. Chim. Acta.* **2004**, *357*, 2503.

Table 1. pK_{a1} Values and β-pyrrole ^{1}H NMR Chemical Shifts of Synthetic Water-Soluble Iron(III) Porphyrins

Iron(III) porphyrin[a]		$(P^{16-})Fe$[d]	$(P^{8-})Fe$[e]	$(TMPS^{4-})Fe$[f]	$(TPPS^{4-})Fe$	$(4\text{-}TMPyP^{4+})Fe$	$(P^{8+})Fe$[h]
***Meso* phenyl substituents**		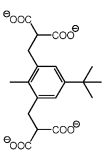	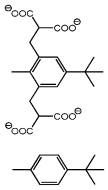				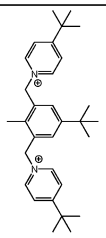
pK_{a1}[b]		9.9	9.3	6.9	7.0	5.5	5.0[h]
β-pyrrole ^{1}H (ppm)[c]	**$(P)Fe^{III}(H_2O)_2$**	45.6	45.6, 46.7	43	52[g]	70[g]	66
	$(P)Fe^{III}(OH)$	80	82	82	NA[g]	NA[g]	83

[a] The quoted charge represents the overall charge on the meso substituents in a given porphyrin ligand. [b] Ref 36. [c] Referenced to TMPS. [d] This work. [e] Ref 5a. [f] Ref 4. [g] Ref 28a, NA = not assigned. [h] Ref 5b.

and 12.7. ^{1}H NMR spectra of complexes of the type $(P)Fe^{III}(L)_n$ (n = 1 and 2) have extensively been analyzed and serve as an excellent means of identification of the product being formed,[28] in which the β-pyrrole proton signal is sensitive to the spin and ligation state of the iron center by hyperfine interaction specially for paramagnetic iron(III) porphyrins. The chemical shift of the β-pyrrole resonance in the purely high-spin state (S = 5/2) iron(III) porphyrin has a value of approximately +80 ppm, characteristic for the (P)Fe−X type (X=OH^-, Cl^-) complex,[25] whereas in the case of pure intermediate spin state (S = 3/2) iron(III) porphyrins, the β-pyrrole ^{1}H resonance moves upfield to approximately −60 ppm. The β-pyrrole resonance in the intermediate spin admixed state (S = 3/2, 5/2) is in between +80 and −60 ppm. Our ^{1}H NMR data indicates a β-pyrrole resonance at +45.6 ppm for pD = 6.5 that shifts downfield to +80 ppm at pD = 12.7. The broad β-pyrrole resonance at +80 ppm at high pH is diagnostic for a monomeric high-spin monohydroxo-ligated iron(III) porphyrin, consistent with the other reported water-soluble ferric porphyrins.[4,5,25] The absence of a β-pyrrole resonance at ∼13 ppm, characteristic for the $((P)Fe^{III})_2O$ dimer, excludes the formation of the μ-oxo-bridged binuclear species at high pH. The observed signal for the diaqua-ligated iron(III) porphyrins exhibits variable $\delta_{\beta-py}$ values in the range from 43−70 ppm, which indicate a varying contribution of S = 3/2 in the spin-admixed mixture (S = 3/2, 5/2) from which it follows that Int % is 24.5 for $(P^{16-})Fe(H_2O)_2$, similar to that found for other $(P^{n-})Fe(H_2O)_2$. The observed data for $(P^{n+})Fe^{III}(H_2O)_2$ shows a marked downfield shift of the β-pyrrole resonance toward the high-spin value with the increasing electron-withdrawing capability of the porphyrin substituents.

Temperature- and pressure-dependent ^{17}O NMR measurements were performed at pH 6.5 (see Figure S1 in Supporting Information) and 12.7. Detailed variable-temperature and -pressure measurements gave the water exchange rate constants (k_{ex}) and activation parameters ($\Delta H^{\ddagger}_{ex}$, $\Delta S^{\ddagger}_{ex}$, and $\Delta V^{\ddagger}_{ex}$). The positive values of $\Delta S^{\ddagger}_{ex} = +66 \pm 10$ J mol^{-1} K^{-1} and $\Delta V^{\ddagger}_{ex} = +6.5 \pm 0.3$ cm^3 mol^{-1} at pH 6.5 support the operation of a dissociative interchange (I_d) mechanism for the water-exchange process on $(P^{16-})Fe^{III}(H_2O)_2$, which is similar to that found for other diaqua-ligated porphyrins (I_d or D).[5,7c] From the analysis of the data, the obtained rate constant for water exchange, $k_{ex} = 4.2 \times 10^6$ s^{-1} at pH 6.5 and 25 °C, is in the similar range of k_{ex} values reported for complexes with negatively charged meso substituents on the porphyrin environment. Conversely, the smaller k_{ex} values determined for the positively charged iron porphyrins of $TMPyP^{4+}$ and P^{8+} suggest that the lability of the metal center is decreased by the influence of the positive porphyrin periphery, thus, stabilizing the $Fe^{III}-H_2O$ bond through an inductive effect. Although there is a trend of increased lability for the P^{16-} and P^{8-} complexes as compared to the $TMPS^{4-}$ complex, the water exchange process for the P^{16-} and P^{8-} complexes is slower than for the $TMPS^{4-}$ complex, which could be attributed to the steric hindrance of the bulky negative carboxylate substituents that prevent the exchange of coordinated water in a dissociative manner. The data obtained for $(P^{16-})Fe^{III}(H_2O)_2$ and related results for other iron(III) porphyrins are summarized in Table 2. In analogous ^{17}O NMR measurements performed at pH 12.7, the bulk $^{17}OH_2$ signal as a function of temperature resulted in only small changes in the line width in the presence and absence of the $(P^{16-})Fe^{III}$, which suggests that $(P^{16-})Fe^{III}$ at high pH forms a five-coordinate monohydroxo-ligated iron porphyrin, $(P^{16-})Fe^{III}(OH)$, that exhibits no measurable water exchange reaction.

Earlier literature reports showed that high-spin monohydroxo-bound iron(III) porphyrins may exist as five-coordinate $(P)Fe^{III}(OH)$ species in non-coordinating solvents or as six-coordinate $(P)Fe^{III}(H_2O)(OH)$ species in aqueous solution as supported by ^{17}O NMR measurements.[4] ^{17}O NMR water exchange studies indicated that no water exchange reaction

(28) (a) Ivanca, M. A.; Lappin, A. G.; Scheidt, W. R. *Inorg. Chem.* **1991**, *30*, 711. (b) La Mar, G. N.; Eaton, G. R.; Holm, R. H.; Walker, F. A. *J. Am. Chem. Soc.* **1973**, *95*, 63. (c) La Mar, G. N.; Walker, F. A. *J. Am. Chem. Soc.* **1973**, *95*, 6950. (d) La Mar, G. N.; Walker, F. A. *J. Am. Chem. Soc.* **1975**, *97*, 5103. (e) Snyder, R. V.; La Mar, G. N. *J. Am. Chem. Soc.* **1976**, *98*, 4419.

Table 2. Rate Constants (at 298 K) and Activation Parameters for Water Exchange Reactions of $(P)Fe^{III}(H_2O)_2$ Complexes

iron(III) porphyrin	Int%[a]	k_{ex} (s^{-1})	$\Delta H^{\ddagger}_{ex}$ (kJ mol^{-1})	$\Delta S^{\ddagger}_{ex}$ (J mol^{-1} K^{-1})	$\Delta V^{\ddagger}_{ex}$ (cm^3 mol^{-1})
$(P^{16-})Fe$[b]	24.5	$(42 \pm 5) \times 10^5$	55 ± 3	$+66 \pm 10$	$+6.5 \pm 0.3$
$(P^{8-})Fe$[c]	24	$(77 \pm 1) \times 10^5$	61 ± 6	$+91 \pm 23$	$+7.4 \pm 0.4$
$(TPPS^{4-})Fe$[d]	20	$(20 \pm 1) \times 10^5$	67 ± 2	$+99 \pm 10$	$+7.9 \pm 0.2$
$(TMPS^{4-})Fe$[e]	26	$(210 \pm 10) \times 10^5$	61 ± 1	$+100 \pm 5$	$+11.9 \pm 0.3$
$(TMPyP^{4+})Fe$[d]	7	$(4.5 \pm 0.1) \times 10^5$	71 ± 2	$+100 \pm 6$	$+7.4 \pm 0.4$
$(P^{8+})Fe$[f]	10	$(5.5 \pm 0.1) \times 10^4$	53 ± 3	$+28 \pm 9$	$+1.5 \pm 0.2$

[a] Contribution of the intermediate spin state ($S = 3/2$) in the spin-admixed $(P)Fe^{III}(H_2O)_2$ porphyrins, compare ref 4b. [b] This work. [c] Ref 5a. [d] Ref 7c. [e] Ref 4. [f] Ref 5b.

was observed for iron porphyrins with negatively charged substituents, although another water molecule could bind to the complex to form $(P^{n-})Fe^{III}(H_2O)(OH)$ in aqueous solution. The observations can be explained in terms of the presence of five-coordinate $(P^{n-})Fe^{III}(OH)$ complexes under such conditions as a result of the strong electron-donating substituents in the porphyrin meso position and the trans labilizing effect of coordinated hydroxide that results in an electron-rich character of the iron(III) center. In contrast, however, $(P^{n+})Fe^{III}(OH)$ complexes with positively charged substituents tend to exist as six-coordinate $(P^{n+})Fe^{III}(H_2O)$-(OH) species such that line-broadening could be observed in the ^{17}O NMR experiments. The latter data are summarized later in the text in Table 6.

It is well established from the ^1H and ^{17}O NMR data summarized in Table 2 that the rates of water exchange correlate with the contribution of the intermediate spin state $S = 3/2$ (Int %) in the spin admixed state ($S = 3/2$, 5/2) of ferric porphyrins, where the contribution of $S = 3/2$ was estimated from the proton β-pyrrole signal.[29] The results show that the calculated Int % value increases with the increasing lability of the water molecule coordinated to the iron(III) center, which is consistent with an increasing water exchange rate (k_{ex}) resulting from the lengthening of the $Fe^{III}-OH_2$ bond. The population of the $S = 3/2$ spin state arises from destabilization of the $d_{x^2-y^2}$ orbital, resulting in an increased electron density on the nitrogens of porphyrin in $(P^{n-})Fe^{III}(H_2O)_2$ as compared to that in $(P^{n+})Fe^{III}(H_2O)_2$. The observed effects also affect the reactivity of the complexes toward NO as will be discussed in more detail later.

Inspection of the structural features reported for 5-coordinate high-spin, 6-coordinate spin-admixed, and 6-coordinate low-spin $(P)Fe^{III}(L)$ systems[8] suggest that minor structural changes are demanded for the formation of $(P)Fe^{II}$-$(H_2O)(NO^+)$ from 6-coordinate $(P)Fe^{III}(H_2O)_2$,[30] in which in both cases the Fe^{III} centers remain in the porphyrin plane. However, NO binding to 5-coordinate $(P)Fe^{III}(OH)$ complexes requires some structural changes as a result of a change in coordination number, which involves movement of the Fe^{III} center from out-of-plane into the porphyrin plane to yield $(P)Fe^{II}(OH)(NO^+)$.

On the basis of the reported spectroscopic results, $(P^{16-})Fe^{III}(H_2O)_2$ represents the six-coordinate spin-admixed ($S = 3/2$, 5/2) species in the range of $6.0 < pH < 9.9$, whereas $(P^{16-})Fe^{III}(OH)$ is predominantly present as a high-spin ($S = 5/2$) five-coordinate complex at pH >9.9 with an out-of-plane metal center toward the OH^- ligand.[31] No indication for the formation of a μ-oxo-bridged dimer or dihydroxo species was found in the pH range studied.

Reaction of $(P^{16-})Fe^{III}(H_2O)_2$ with Nitric Oxide. When gaseous NO is added to a solution of $(P^{16-})Fe^{III}(H_2O)_2$, rapid spectral changes occur as shown in Figure 3, indicating the formation of a typical low-spin iron nitrosyl complex in which electron transfer from NO to Fe(III) produces $(P^{16-})Fe^{II}(H_2O)(NO^+)$. The maximum of the Soret- and Q-bands shifts from 398 and 532 nm to 428 ($\epsilon = 9.8 \times 10^4$ M^{-1} cm^{-1}) and 541 nm ($\epsilon = 1.3 \times 10^4$ M^{-1} cm^{-1}), respectively, during formation of the final product according to reaction 5. The binding of NO appears to be reversible as

$$(P^{16-})Fe^{III}(H_2O)_2 + NO \underset{k_{off}}{\overset{k_{on}}{\rightleftharpoons}} (P^{16-})Fe^{II}(H_2O)(NO^+) + H_2O \quad K_{NO} = k_{on}/k_{off} \quad (5)$$

determined from an experiment in which the bubbling of an inert gas through the product shifted the equilibrium back to the reactant side. The thermodynamic equilibrium constant, $K_{NO} = (1.7 \pm 0.2) \times 10^5$ M^{-1} was determined from the spectral changes observed for various NO concentrations measured in solution with an NO electrode, as shown in the inset of Figure 3.[5]

The kinetics for the reversible binding of NO were investigated by stopped-flow technique for the "on" and "off" reaction, respectively. The observed reaction proved to be follow pseudo-first-order kinetics with an at least 10-fold excess of NO, and the observed rate constant, k_{obs}, is expressed by eq 6. Accordingly, k_{obs} depends linearly on

$$k_{obs} = k_{on}[NO] + k_{off} \quad (6)$$

[NO] with a slope of $k_{on} = (33.6 \pm 0.5) \times 10^4$ M^{-1} s^{-1} and an intercept of $k_{off} = 4 \pm 3$ s^{-1} at 14.7 °C. The values of k_{off}

(29) Ikezaki, A.; Nakamura, M. *Inorg. Chem.* **2002**, *41*, 6225.
(30) (a) Scheidt, W. R.; Reed, Ch. A. *Chem. Rev.* **1981**, *81*, 543. (b) Simonato, J.-P.; Pecaut, J.; Le pape, L.; Oddou, J.-L.; Jeandey, C.; Shang, M. R.; Wojaczynski, J.; Wolowiec, S.; Latos-Grazynski, L.; Marchon, J.-C. *Inorg. Chem.* **2000**, *39*, 3978. (c) Cheng, B.; Scheidt, W. R. *Acta Crystallogr., Sect. C: Cryst. Struct. Commun.* **1995**, *57*, 1271. (d) Safo, M. K.; Schmidt, W. R.; Grupa, G. P.; Orosz, R. D.; Reed, Ch. A. *Inorg. Chim. Acta.* **1991**, *184*, 251. (e) Körber, F. C. F.; Linsay Smith, J. R.; Prince, S.; Rizkallah, P.; Reynolds, C. D.; Shawcross, D. R. *J. Chem. Soc., Dalton Trans.* **1991**, 3291.
(31) (a) Swepston, P. N.; Ibers, J. A. *Acta Crystallogr., Sect. C: Cryst. Struct. Commun.* **1985**, *41*, 671. (b) Hoffman, A. B.; Collins, D. M.; Day, V. W.; Fleischer, E. B.; Srivastava, R. S.; Hoard, J. L. *J. Am. Chem. Soc.* **1972**, *94*, 3620.

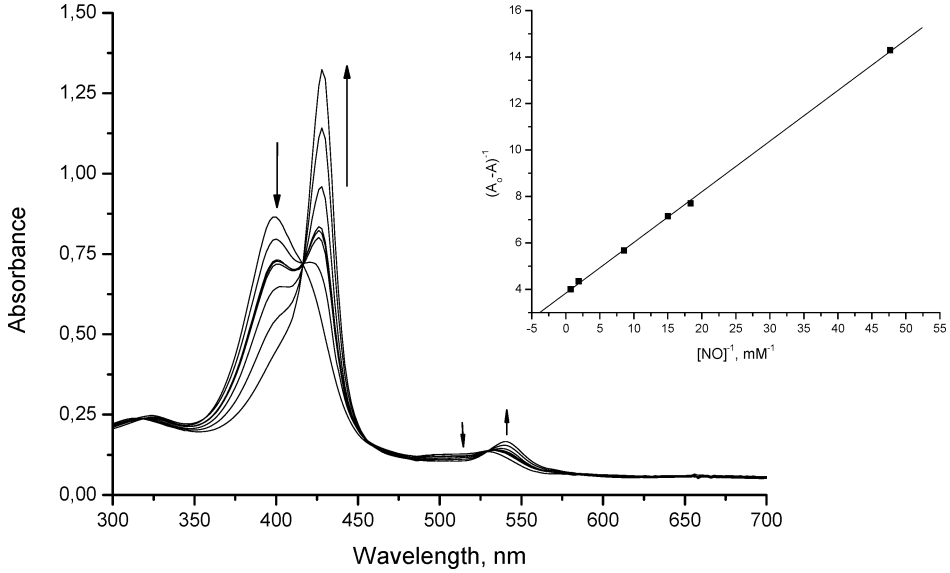

Figure 3. Spectral changes recorded for the binding of NO to $(P^{16-})Fe^{III}(H_2O)_2$. The inset shows a plot of $(A - A_0)^{-1}$ versus $[NO]^{-1}$ (where A_0 = absorbance at 398 nm at [NO] = 0 and A= absorbance at 398 nm at a given NO concentration). Experimental conditions: $[(P^{16-})Fe^{III}] = 1.34 \times 10^{-5}$ M, pH = 6.5 (0.05M Mes), temp = 25 °C, I = 0.1 M (with $NaClO_4$)

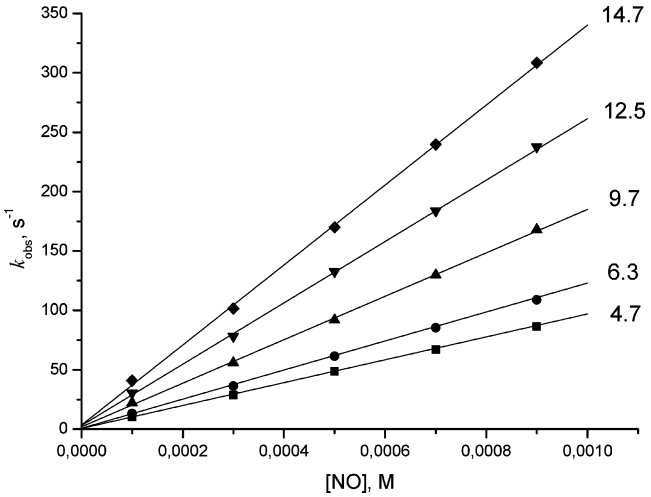

Figure 4. Plots of k_{obs} versus [NO] for the reaction of $(P^{16-})Fe^{III}(OH_2)_2$ with NO in the restricted temperature range of 4.7−14.7 °C measured with the stopped-flow technique. Experimental conditions: $[(P^{16-})Fe^{III}] = 2.0 \times 10^{-5}$ M, pH 6.5 (0.05 M Mes), λ_{det} = 430 nm, I = 0.1 M (with $NaClO_4$).

Table 3. Rate and Activation Parameters for the Binding and Release of NO to $(P^{16-})Fe^{III}(H_2O)_2$ at pH 6.5 by Stopped-Flow and NO-Trapping Methods

temp (°C)	pressure (MPa)	k_{on} ($\times 10^4$ M^{-1} s^{-1})	k_{off} (s^{-1})	k_{off} [a] (s^{-1})
4.7	0.1	9.6 ± 0.2	0.6 ± 0.4	2.3 ± 0.2
6.3	0.1	12.2 ± 0.4	0.9 ± 0.5	3.2 ± 0.2
9.7	0.1	18.3 ± 0.3	2 ± 1	6.1 ± 0.1
12.5	0.1	25.9 ± 0.3	3 ± 2	10.1 ± 0.1
14.7	0.1	33.6 ± 0.5	4 ± 3	13.7 ± 0.3
20	0.1			31.4 ± 0.2
25	0.1			65.5 ± 0.5
2.5	10	10.5 ± 0.3		1.7 ± 0.1
	50	8.6 ± 0.4		1.3 ± 0.1
	90	7.0 ± 0.4		1.0 ± 0.1
	130	5.9 ± 0.5		0.7 ± 0.1
$\Delta H^{\ddagger}$ (kJ mol^{-1})		80 ± 1	117 ± 13	110 ± 2
$\Delta S^{\ddagger}$ (J mol^{-1} K^{-1})		+138 ± 4	+173 ± 24	+161 ± 8
$\Delta V^{\ddagger}$ (cm^3 mol^{-1})		+10.8 ± 0.2		+16.9 ± 0.3

[a] Data obtained by the NO-trapping method with the use of $[Ru^{III}(edta)(H_2O)]^-$, compare to Figure S3 (Supporting Information).

are small and subjected to large error limits when determined by extrapolation of plots of k_{obs} versus [NO] to [NO] = 0. More reliable k_{off} values were obtained in a direct way by using an NO trap, namely, $[Ru^{III}(edta)(H_2O)]^-$, an efficient scavenger for NO. Fast NO trapping by an excess of scavenger from $(P^{16-})Fe^{II}(H_2O)(NO^+)$ gives the original complex $(P^{16-})Fe^{III}(H_2O)_2$ and $[Ru^{III}(edta)(NO)]^-$, as indicated by the observed spectral changes. The kinetic traces were recorded at 430 nm and could be fitted with a single-exponential function. The rate constant for NO release is the rate-limiting step under the selected conditions (see reaction 7) since the observed rate constant does not depend on the concentration of $[Ru^{III}(edta)(H_2O)]^-$ employed since it is a much faster reaction than either k_{on} or k_{off}. The values of k_{off} determined in this way differ considerably from those extrapolated from the data in Figure 4, as shown in Table 3. The overall equilibrium constant obtained from the kinetic data, $K_{NO} = k_{on}/k_{off} = (1.7 \pm 0.1) \times 10^5$ M^{-1} at 25 °C, is in an excellent agreement with the thermodynamic value of K_{NO} determined from spectral changes as a function of [NO], namely, $(1.7 \pm 0.2) \times 10^5$ M^{-1}.

$$\begin{array}{l} (P^{16-})Fe^{II}(H_2O)(NO^+) + H_2O \\ \qquad k_{off} \;\big\downarrow\big\uparrow\; k_{on} \\ (P^{16-})Fe^{III}(H_2O)_2 \;+\; NO \\ \qquad\qquad \big\downarrow\; [Ru^{III}(edta)(H_2O)]^- \\ [Ru^{III}(edta)(NO)]^- \;+\; H_2O \end{array} \qquad (7)$$

The binding (k_{on}) and release of NO (k_{off}) rate constants were determined as a function of temperature in the restricted range of 4.7−14.7 °C because of the limitations of the stopped-flow technique (see Table 3 and Figure 4). Eyring plots (see Figures S2 and S3, in Supporting Information) were constructed from which the activation parameters, $\Delta H^{\ddagger}$

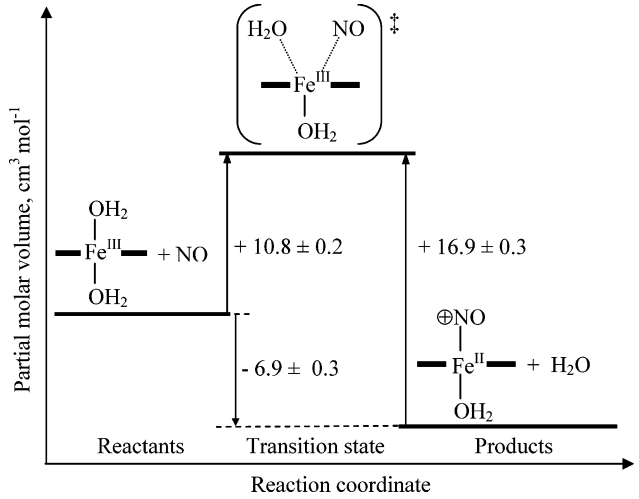

Figure 5. Volume profile for the reversible binding of nitric oxide to $(P^{16-})Fe^{III}(H_2O)_2$ according to reaction 5.

and $\Delta S^{\ddagger}$ for the *on* and *off* reactions, were determined. Despite the large difference in the k_{off} values, the calculated activation parameters, $\Delta H^{\ddagger}_{off}$ and $\Delta S^{\ddagger}_{off}$, obtained with the stopped-flow and NO-trapping techniques are rather similar and do not affect the mechanistic interpretation. For a better understanding of the underlying reaction mechanism, activation volumes were determined from the effect of pressure up to 130 MPa on k_{on} and k_{off} (see Figure S4 in Supporting Information) and are included in Table 3. The reported activation volumes were used to construct a volume profile for reaction 5 as shown in Figure 5. The obtained rate and activation parameters are summarized in comparison with other $(P)Fe^{III}(H_2O)_2$ complexes in Table 4.

Reaction of $(P^{16-})Fe^{III}(OH)$ with Nitric Oxide. As reported in our earlier papers,[5] spectroscopic and kinetic studies on the reaction of NO with iron(III) porphyrins at pH $\gg$ pK_a indicate that the nature of the resulting nitrosyl species and the NO binding mechanism differ from those observed for the diaqua-ligated iron porphyrins. Figure 6 shows the spectral changes that accompany the reaction of $(P^{16-})Fe^{III}(OH)$ with NO at pH 12.7, where the decrease in the absorbance maximum at 418 nm is accompanied by the appearance of new bands at 433 ($\epsilon = 9.7 \times 10^4$ M^{-1} cm^{-1}) and 547 nm ($\epsilon = 1.2 \times 10^4$ M^{-1} cm^{-1}) for the formation of the nitrosyl product, $(P^{16-})Fe^{II}(OH)(NO^+)$. The latter UV−vis spectrum differs from that observed for the corresponding reaction at low pH (viz., 428 and 541 nm at pH 6.5) and points to the formation of a deprotonated form of the nitrosyl product at high pH as given in eq 8.

$$(P^{16-})Fe^{III}(OH) + NO \underset{k_{off}}{\overset{k_{on}}{\rightleftharpoons}} (P^{16-})Fe^{II}(OH)(NO^+) \qquad K_{NO} = k_{on}/k_{off} \quad (8)$$

For the reversible binding of NO to $(P^{16-})Fe^{III}(OH)$ at pH 12.7, $K_{NO} = (4.1 \pm 0.4) \times 10^3$ M^{-1} at 25 °C was determined from the spectral changes as a function of the [NO] shown in Figure 6.[4] Detailed kinetic measurements for the reversible binding of NO to $(P^{16-})Fe^{III}(OH)$ were carried out in a manner similar to that employed for $(P^{16-})Fe^{III}(H_2O)_2$. $k_{on} = (31.5 \pm 0.2) \times 10^3$ M^{-1} s^{-1} and $k_{off} = 8.0 \pm 0.1$ s^{-1} at 25 °C were obtained from the slope and intercept of a linear plot of k_{obs} versus [NO], respectively. The thermodynamic equilibrium constant is close to the value calculated from the kinetic data, namely, $K_{NO} = k_{on}/k_{off} = (3.9 \pm 0.2) \times 10^3$ M^{-1} at 25 °C. Variable-temperature and -pressure experiments were performed to determine the activation parameters in a manner similar to that for the diaqua complex. The results are reported in Table 5 and Figures 7, S5, and S6 and are compared with a series of related systems in Table 6. The reported activation volumes for the *on* and *off* reactions were used to construct the volume profile reported in Figure 8.

As mentioned above, the spectra reported in Figure 9a show differences for the nitrosyl product formed at pH 6.5 and 12.7. The plot of absorbance at 434 nm versus pH in Figure 9b, fitted with a sigmoidal function, resulted in p$K_{a(NO)} = 9.68 \pm 0.03$ for the deprotonation of a coordinated water molecule in the nitrosyl product $(P^{16-})Fe^{II}(NO^+)(H_2O)$ as given in reaction 9. The observed reactions can be summarized as outlined in Scheme 2.

$$(P^{16-})Fe^{II}(NO^+)(H_2O) \rightleftarrows (P^{16-})Fe^{II}(NO^+)(OH^-) + H^+ \qquad pK_{a(NO)} = 9.68 \quad (9)$$

In comparison to the binding and release rate constants at pH 6.5 (viz., 1.84×10^5 M^{-1} s^{-1} and 6.1 s^{-1}, at 10 °C, see Table 3) the corresponding values at pH 12.7 and 10 °C are 1.91×10^4 M^{-1} s^{-1} and 1.0 s^{-1}, respectively, indicating that both NO binding and release rates for $(P^{16-})Fe^{III}(OH)$ are significantly slower than those for $(P^{16-})Fe^{III}(H_2O)_2$. A

Table 4. Rate Constants (at 298 K) and Activation Parameters for Reversible Binding of NO to a Series of Diaqua-Ligated Water Soluble Iron(III) Porphyrins

			NO binding				NO release			
iron(III) porphyrin	pK_{a1}	Int %	k_{on} ($\times 10^4$ M^{-1} s^{-1})	$\Delta H^{\ddagger}_{on}$ (kJ mol^{-1})	$\Delta S^{\ddagger}_{on}$ (J mol^{-1} K^{-1})	$\Delta V^{\ddagger}_{on}$ (cm^3 mol^{-1})	k_{off} (s^{-1})	$\Delta H^{\ddagger}_{off}$ (kJ mol^{-1})	$\Delta S^{\ddagger}_{off}$ (J mol^{-1} K^{-1})	$\Delta V^{\ddagger}_{off}$ (cm^3 mol^{-1})
$(P^{16-})Fe^a$	9.8	24.5	113 ± 5^f	80 ± 1	$+138 \pm 4$	$+10.8 \pm 0.2$	22 ± 3	117 ± 13	$+173 \pm 24$	
							65.5 ± 0.5^g	110 ± 2^g	$+161 \pm 8^g$	$+16.9 \pm 0.3^g$
$(P^{8-})Fe^b$	9.3	24	82 ± 1	51 ± 1	$+40 \pm 2$	$+6.1 \pm 0.1$	220 ± 2	101 ± 2	$+140 \pm 7$	$+16.8 \pm 0.4$
$(TMPS^{4-})Fe^c$	6.9	26	280 ± 20	57 ± 3	$+69 \pm 11$	$+13 \pm 1$	900 ± 200	84 ± 3	$+94 \pm 10$	$+17 \pm 3$
$(TPPS^{4-})Fe^c$	7.0	20	50 ± 3	69 ± 3	$+95 \pm 10$	$+9 \pm 1$	500 ± 400	76 ± 6	$+60 \pm 11$	$+18 \pm 2$
$(TMPyP^{4+})Fe^d$	5.5	7	2.9 ± 0.2	67 ± 4	$+67 \pm 13$	$+3.9 \pm 1.0$	59 ± 4	108 ± 5	$+150 \pm 12$	$+16.6 \pm 0.2$
$(P^{8+})Fe^e$	5.0	10	1.5 ± 0.1	77 ± 3	$+94 \pm 12$	$+1.5 \pm 0.3$	26.3 ± 0.5	83 ± 4	$+61 \pm 14$	$+9.3 \pm 0.5$

[a] This work. [b] Ref 5a. [c] Ref 3d. [d] Ref 6a. [e] Ref 5b. [f] Calculated for 298 K from Eyring plots based on data from Table 3. [g] Data measured with $[Ru^{III}(edta)(H_2O)]^-$ as NO scavenger.

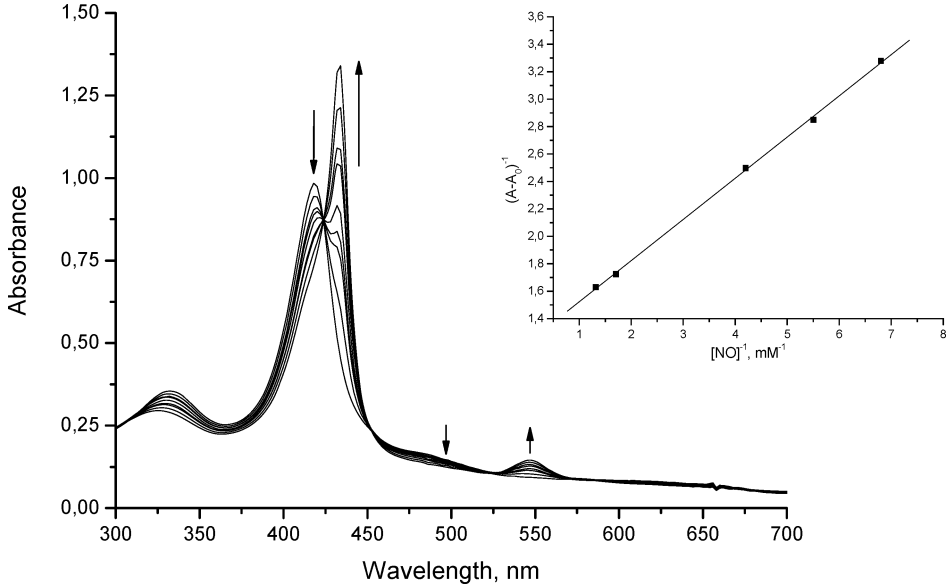

Figure 6. Spectral changes resulting from the binding of NO to $(P^{16-})Fe^{III}(OH)$. The inset shows a plot of $(A - A_0)^{-1}$ versus $[NO]^{-1}$ (where A_0 = absorbance at 435 nm at [NO] = 0 and A = absorbance at 435 nm at a given NO concentration). Experimental conditions: $[(P^{16-})Fe^{III}] = 1.38 \times 10^{-5}$ M, pH = 12.7 (0.05M NaOH), temp = 25 °C, I = 0.1 M (with $NaClO_4$).

Table 5. Rates and Activation Parameters for the Binding and Release of NO for $(P^{16-})Fe^{III}(OH)$ at pH 12.7 by Stopped-Flow and NO-Trapping Methods

temp (°C)	pressure (MPa)	k_{on} ($\times 10^3$ M^{-1} s^{-1})	k_{off} (s^{-1})	k_{off}[a] (s^{-1})
5	0.1	14.8 ± 0.2	0.32 ± 0.04	0.6 ± 0.1
10	0.1	19.1 ± 0.9	1.1 ± 0.1	1.0 ± 0.1
15	0.1	21.8 ± 0.5	2.0 ± 0.3	1.8 ± 0.1
20	0.1	26.3 ± 1.2	4.1 ± 0.6	2.9 ± 0.1
25	0.1	31.5 ± 0.2	8.0 ± 0.1	4.8 ± 0.1
2.5	10	4.5 ± 0.2		0.33 ± 0.04
	50	5.3 ± 0.3		0.25 ± 0.03
	90	6.3 ± 0.5		0.19 ± 0.02
	130	7.4 ± 0.4		0.15 ± 0.03
$\Delta H^{\ddagger}$ (kJ mol^{-1})		23 ± 1	108 ± 7	84 ± 1
$\Delta S^{\ddagger}$ (J mol^{-1} K^{-1})		−82 ± 4	+136 ± 19	+53 ± 4
$\Delta V^{\ddagger}$ (cm^3 mol^{-1})		−9.4 ± 0.2		+15 ± 1

[a] Data obtained by the NO-trapping method with the use of $[Ru^{III}(edta)(H_2O)]^-$ as a trap for NO (see Figures S5 and S6).

comparison of these rate constants along with those for a series of complexes studied before is given in Table 7. From the data shown in Figure 10a, it can be seen that the rates of NO binding as a function of pH in the range of 6.5−12.7 resulted in k_{on} values that decrease with increasing pH (see Figure 10b). A fit of the data resulted in a pK_a value of 9.83 ± 0.03, which is similar to that determined from a spectrophotometric titration (viz., pK_{a1} = 9.90), suggesting that the rate of NO binding is controlled by the axial ligand bound to the metal center and reflects differences in the kinetics of NO binding at low and high pH. In the case of NO dissociation rates, the k_{off} values are rather small and include large errors when extrapolated from plots of k_{obs} versus [NO]. More reliable values were obtained for k_{off} using the NO-trapping method mentioned above. A similar observation was shown previously for other water-soluble iron(III) porphyrins.

Spectroscopic and Kinetic Studies on the Subsequent Reactions. The nitrosyl complex $(P^{16-})Fe^{II}(H_2O)(NO^+)$ at pH 6.5 undergoes a subsequent reaction on a longer time scale in which the characteristic bands at 428 and 541 nm disappear with a concomitant appearance of new bands at 416 and 612 nm, respectively (see Figure 11). The obtained kinetic trace for this reaction can be fitted with a single-exponential function as shown in the inset of Figure 11. The final spectrum resembles that of a five-coordinate ferrous nitrosyl product and is the same as that observed for the product formed in the reaction of NO with reduced $(P^{16-})Fe^{II}$. This suggests that $(P^{16-})Fe^{II}(H_2O)(NO^+)$ is converted to $(P^{16-})Fe^{II}(NO)$ by a slow redox process as outlined in reactions 10−12. The observed spectral changes are similar to that reported for other negatively charged water-soluble iron(III) porphyrins.[17,18]

$$(P^{16-})Fe^{III}(H_2O)_2 + NO \overset{K_{NO}}{\rightleftharpoons} (P^{16-})Fe^{II}(H_2O)(NO^+) + H_2O \quad (10)$$

$$(P^{16-})Fe^{II}(H_2O)(NO^+) \xrightarrow[+H_2O]{k_{red}} (P^{16-})Fe^{II}(H_2O) + NO_2^- + 2H^+ \quad (11)$$

$$(P^{16-})Fe^{II}(H_2O) + NO \xrightarrow{fast} (P^{16-})Fe^{II}(NO) + H_2O \quad (12)$$

The effect of the NO concentration on the observed reductive nitrosylation reaction at pH 6.5 and 25 °C is reported in Figure 12a, from which it follows that k_{obs} increases with increasing [NO] in a nonlinear way and reaches a constant value at high [NO]. In agreement with the rate law (eq 13) for the above given reaction scheme, the plot of k_{obs}^{-1} vs $[NO]^{-1}$ is linear as displayed in Figure 12b, from which the values for K_{NO} and k_{red} were calculated to be (1.4 ± 0.2) × 10^5 M^{-1} and (1.7 ± 0.3) × 10^{-4} s^{-1}, respectively. This value for K_{NO} is close to the equilibrium constant calculated from the kinetic data, namely, $K_{NO} = k_{on}/k_{off}$ = (1.7 ± 0.1) × 10^5 M^{-1} at 25 °C, and the value of

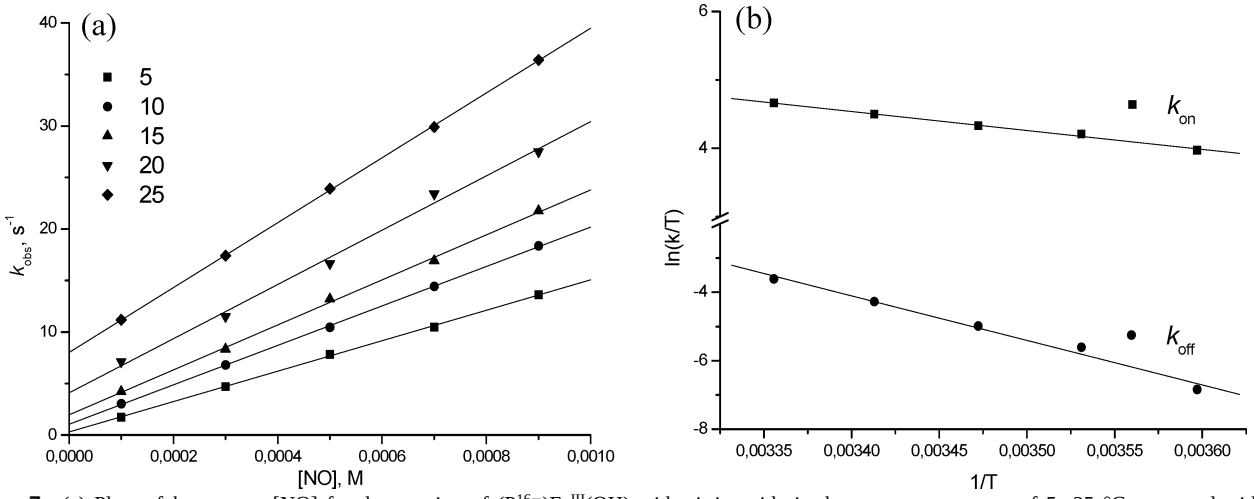

Figure 7. (a) Plots of k_{obs} versus [NO] for the reaction of $(P^{16-})Fe^{III}(OH)$ with nitric oxide in the temperature range of 5−25 °C measured with the stopped-flow technique. (b) Corresponding Eyring plots for the *on* and *off* reactions. Experimental conditions: $[(P^{16-})Fe^{III}] = 2.0 \times 10^{-5}$ M, pH 12.7 (0.05 M NaOH), $\lambda_{det} = 435$ nm, $I = 0.1$ M (adjusted with $NaClO_4$).

Table 6. Rate Constants (at 298 K) and Activation Parameters for Water Exchange and Reversible Binding of NO to Monohydroxo-ligated Iron(III) Porphyrins

		NO binding				NO release			
iron(III) porphyrin	k_{ex} ($\times 10^5$ s^{-1})	k_{on} ($\times 10^4$ M^{-1} s^{-1})	$\Delta H^{\ddagger}_{on}$ (kJ mol^{-1})	$\Delta S^{\ddagger}_{on}$ (J mol^{-1} K^{-1})	$\Delta V^{\ddagger}_{on}$ (cm^3 mol^{-1})	k_{off} (s^{-1})	$\Delta H^{\ddagger}_{off}$ (kJ mol^{-1})	$\Delta S^{\ddagger}_{off}$ (J mol^{-1} K^{-1})	$\Delta V^{\ddagger}_{off}$ (cm^3 mol^{-1})
$(P^{16-})Fe^a$	*e*	3.1 ± 0.4	23 ± 1	−82 ± 4	−9.4 ± 0.2	8.0 ± 0.1	108 ± 7	+136 ± 19	
						7.1 ± 0.1[h]	84 ± 1[h]	+53 ± 4[h]	+15 ± 1[h]
$(P^{8-})Fe^b$	*e*	5.1 ± 0.2	34.6 ± 0.4	−39 ± 1	−6.1 ± 0.2	11.4 ± 0.3[i]	107 ± 2	+136 ± 7	+17 ± 3
$(TMPS^{4-})Fe^c$	*f*	1.46 ± 0.02	28.1 ± 0.6	−128 ± 2	−16.2 ± 0.4	10.5 ± 0.2[j]	90 ± 1	+77 ± 3	+7.4 ± 1.0
$(TMPyP^{4+})Fe^d$	*g*	0.36 ± 0.01	41.4 ± 0.5	−38 ± 5	−13.7 ± 0.6	3.2 ± 0.1	78 ± 2	+25 ± 7	+9.5 ± 0.8
$(P^{8+})Fe^d$	24 ± 6	0.16 ± 0.01	41 ± 1	−45 ± 2	−13.8 ± 0.4	6.2 ± 0.1	72 ± 2	+12 ± 5	+2.6 ± 0.2

[a] This work. [b] Ref 5a. [c] Ref 4. [d] Ref 5b. [e] No water exchange process was detected, compare ref 5a. [f] Although the effect of $(TMPS^{4-})Fe^{III}(OH)$ on the bulk water line width is observable in temperature dependent ^{17}O NMR studies, it was too small to determine k_{ex} and the corresponding activation parameters for the water exchange reaction, compare ref 4. [g] Formation of a μ-oxo dimer at porphyrin concentrations required for NMR measurements precludes reliable studies on the water exchange process. [h] Data measured with $[Ru^{III}(edta)(H_2O)]^-$ as a scavenger for NO. [i] At 297 K. [j] Calculated for 298 K from the Eyring plots, compare ref 5b.

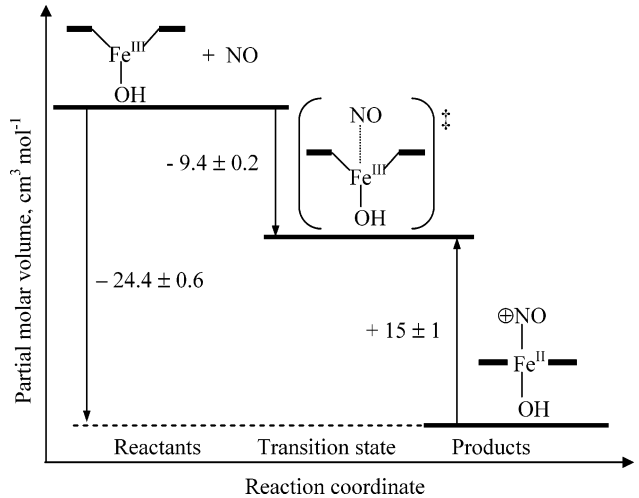

Figure 8. Volume profile for the reversible binding of nitric oxide to $(P^{16-})Fe^{III}(OH)$ according to reaction 8.

k_{red} is in a good agreement with that measured directly at high [NO], namely, $k_{obs} = 1.56 \times 10^{-4}$ s^{-1}.

$$k_{obs} = \frac{k_{red}K_{NO}[NO]}{1 + K_{NO}[NO]} \quad (13)$$

The observed value for k_{red} for $(P^{16-})Fe^{II}(H_2O)(NO^+)$ is the smallest among the series of water-soluble iron porphyrins $(P)Fe^{III}$ as summarized in Table 9. In general, slow reduction rates are observed for the negatively charged complexes with values for k_{red} of approximately 10^{-4} s^{-1} at 25 °C. In contrast, the positively charged porphyrins show a much faster reductive nitrosylation, which suggests that the nucleophilicity of coordinated NO^+ on the Fe^{II} center is affected by the porphyrin environment in controlling the stability of the intermediate $(P^n)Fe^{II}(H_2O)(NO^+)$, which affects the rate of the subsequent redox reaction.

The observed reductive nitrosylation reaction is catalyzed by nitrite and was systematically studied as a function of pH, nitrite concentration, temperature, and pressure. The suggested sequence for the nitrite-catalyzed reaction is given in reaction 14, for which the observed rate constant can be expressed as shown in eq 15.

$$(P^{16-})Fe^{III} + NO \overset{K_{NO}}{\rightleftharpoons} (P^{16-})Fe^{II}(NO^+) + NO_2^- \xrightarrow{k_{nit}} (P^{16-})Fe^{II}(NO) + \text{other products} \quad (14)$$

$$k_{obs} = \frac{k_{nit}K_{NO}[NO_2^-][NO]}{1 + K_{NO}[NO]} \quad (15)$$

The observed rate constant shows a linear dependence on the nitrite concentration as shown in Figure 13 for which the second-order rate constant is $(1.3 \pm 0.2) \times 10^{-2}$ M^{-1}

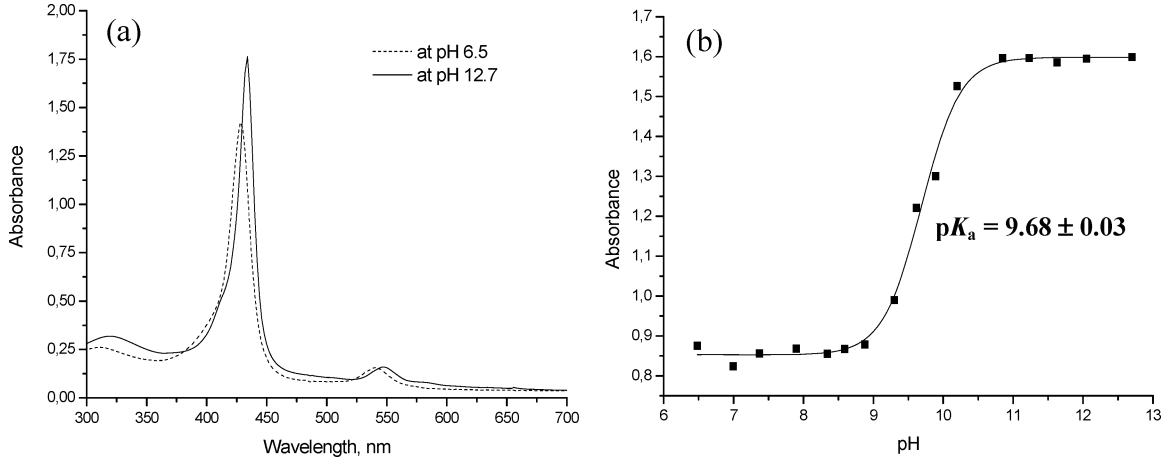

Figure 9. (a) Spectral changes accompanying the reaction of $(P^{16-})Fe^{III}$ with NO at pH 6.5 and 12.7. (b) A plot of absorbance at 434 nm versus pH in buffered aqueous solutions in the pH range of 6.5−12.7. Experimental conditions: $[(P^{16-})Fe^{III}] = 7 \times 10^{-5}$ M, [NO] = 1 mM, temp = 25 °C, I = 0.1 M (with $NaClO_4$). Buffers: pH 6.5, 0.05 M Mes; pH 7, 0.05 M Bis-Tris; pH 7.5−8.8, 0.05 M Taps; pH 9.1, 0.05 M borate; pH 9.5−11.6, 0.05 M Caps; pH 12.0−12.7, NaOH.

Scheme 2

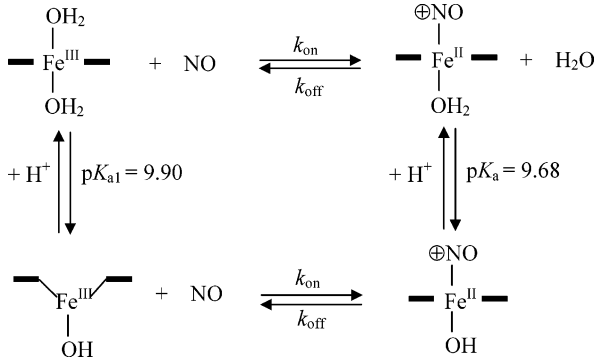

Table 7. Ratio of Rate Constants Observed for the NO Binding ($k_{on}^{H_2O}/k_{on}^{OH}$) and Release ($k_{off}^{H_2O}/k_{off}^{OH}$) for Selected Water-Soluble Iron(III) Porphyrins

(P)Fe^{III}	Int %	$k_{on}^{H_2O}/k_{on}^{OH}$	$k_{off}^{H_2O}/k_{off}^{OH}$
(P^{16-})Fe	24.5	36	9.1
(P^{8-})Fe	24	16	19.3
$(TMPS^{4-})$Fe	26	192	85
$(TMPyP^{4+})$Fe	7	8.0	18.4
(P^{8+})Fe	10	9.4	4.2

s^{-1}, which presents $k_{nit}K_{NO}[NO]/(1 + K_{NO}[NO])$. Since K_{NO} and [NO] are known under the selected experimental conditions, the values of k_{obs} could be converted to the corresponding k_{nit} values (summarized in Table 8) as a function of temperature and pressure at pH 6.5. The activation parameters were estimated in the usual way for which the corresponding plots are reported in Figure S7 (Supporting Information). The results are summarized along with the rate constants and activation parameters for the other investigated complexes in Table 9. On the basis of these data, the nitrite-induced reductive nitrosylation is the slowest for $(P^{16-})Fe^{II}(H_2O)(NO^+)$ in comparison to all other studied porphyrins, suggesting that the overall negative charge reduces the electrophilicity of the coordinated NO^+ and slows down the direct binding of NO_2^-.

The observed reaction is also catalyzed by hydroxide ions. The $[OH^-]$ dependence of the reductive nitrosylation reaction is reported in Figure S8 (Supporting Information), in which

Table 8. Effect of Temperature and Pressure on the Nitrite-Induced Reductive Nitrosylation Reaction of $(P^{16-})Fe^{II}(H_2O)(NO^+)$ with Nitrite Ion at pH 6.5[a]

temp (°C)	pressure (MPa)	$10^3\,k_{obs}$ (s^{-1})	$10^2\,k_{nit}$ ($M^{-1}\,s^{-1}$)
25	0.1	0.22 ± 0.02	1.4 ± 0.1
30	0.1	0.37 ± 0.04	2.5 ± 0.3
35	0.1	0.58 ± 0.05	4.1 ± 0.4
40	0.1	1.09 ± 0.05	8.1 ± 0.5
45	0.1	1.53 ± 0.07	11.9 ± 0.5
27	10	0.33 ± 0.06	2.2 ± 0.3
	50	0.39 ± 0.05	2.7 ± 0.5
	90	0.45 ± 0.06	3.1 ± 0.4
	130	0.54 ± 0.07	3.6 ± 0.7
$\Delta H^{\ddagger}$ (kJ mol^{-1})			80.4 ± 1.4
$\Delta S^{\ddagger}$ (J $mol^{-1}\,K^{-1}$)			−10.8 ± 3.1
$\Delta V^{\ddagger}$ (cm^3 mol^{-1})			−9.8 ± 0.4

[a] $[NO_2^-]$ = 16 mM

the observed reaction was studied in the pH range of 6.0−8.4 where a water molecule is still bound to the metal center. Since the plot gives a straight line with a nonzero intercept, k_{obs} can be formulated as given in eq 16.

$$k_{obs} = k_{OH}[OH^-] + k_{H_2O} \qquad (16)$$

The obtained slope and intercept of the plot are $k_{OH} = 1.0 \times 10^3\ M^{-1}\,s^{-1}$ and $k_{H_2O} = 1.1 \times 10^{-4}\ s^{-1}$, respectively. The value of k_{OH} is consistent with that measured for metalloproteins and the ferric heme complex, $(P^{8-})Fe^{II}(H_2O)(NO^+)$, for which analogous measurements resulted in $k_{OH} = 4.5 \times 10^3\ M^{-1}\,s^{-1}$ and $k_{H_2O} = 1.1 \times 10^{-4}\ s^{-1}$, respectively.[3,6] This means that OH^- and H_2O, as well as NO_2^-, contribute to the reductive nitrosylation of $(P^{16-})Fe^{II}(H_2O)(NO^+)$ to yield $(P^{16-})Fe^{II}$ species. The base-catalyzed reaction is much more effective than the nitrite-catalyzed reaction as shown by $k_{OH} = 1.0 \times 10^3\ M^{-1}\,s^{-1}$ and $k_{nit} = (1.3 \pm 0.2) \times 10^{-2}\ M^{-1}\,s^{-1}$, respectively.

The overall reaction is accompanied by an electron-transfer process in which $(P^{16-})Fe^{II}(NO)$ is formed from $(P^{16-})Fe^{II}(NO^+)$. Potential measurements using cyclic voltammetry resulted in an irreversible $\Delta E_{1/2}((P^{16-})Fe^{II}-NO^+/(P^{16-})Fe^{II}-NO)$ of 0.20 V versus Ag/AgCl at pH 6.5. This value fits

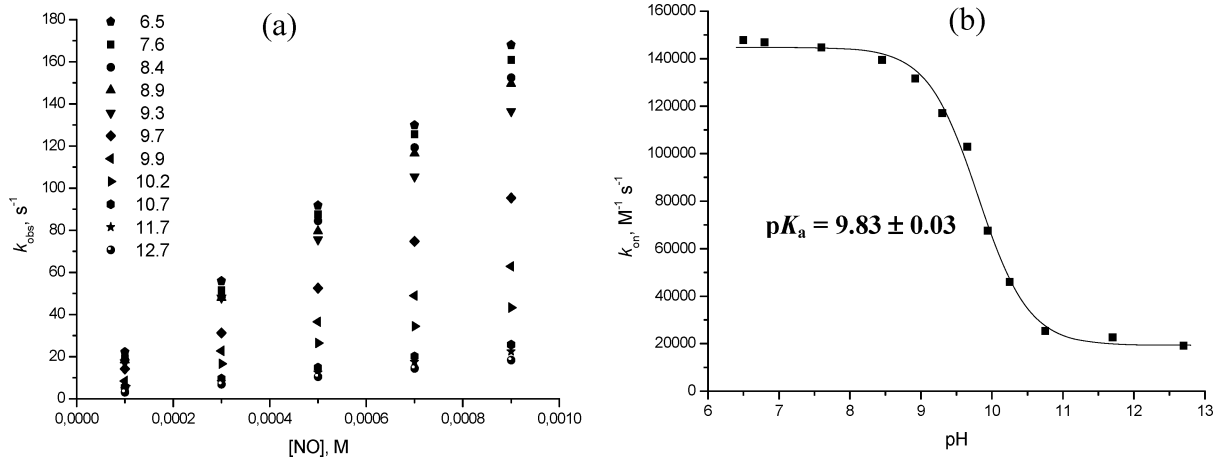

Figure 10. (a) pH dependence of the rate constants for the reaction of NO with $(P^{16-})Fe^{III}$. (b) Plots of k_{on} versus pH, where k_{on} was determined from the slopes of k_{obs} versus [NO] plots measured in the pH range of 6.5−12.7. Experimental conditions: $[(P^{16-})Fe^{III}] = 2.0 \times 10^{-5}$ M, temp = 10 °C, $\lambda_{det} = 435$ nm, $I = 0.1$ M (with $NaClO_4$).

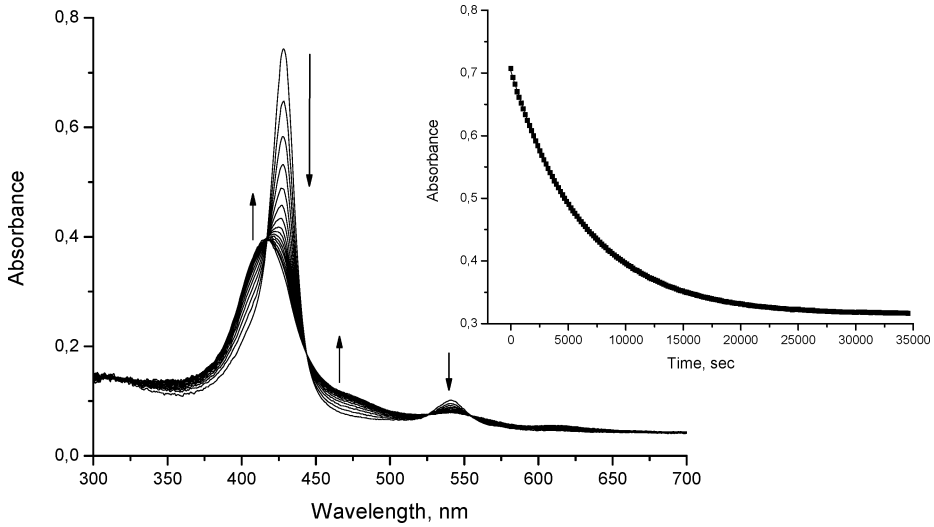

Figure 11. Spectral changes observed during the subsequent reaction following the binding of NO to $(P^{16-})Fe^{III}(H_2O)_2$. The inset shows the kinetic trace of absorbance versus time fitted to a single-exponential function. Experimental conditions: $[(P^{16-})Fe^{III}] = 1 \times 10^{-5}$ M, [NO] = 1 mM, pH = 6.5 (0.05M Mes), $\lambda_{det} = 431$ nm, temp = 25 °C, $I = 0.1$ M with $NaClO_4$. The first ten spectra were recorded every 6 min, the next 10 spectra every 9 min, and the rest every 15 min to give $k_{obs} = 1.56 \times 10^{-4}$ s^{-1}.

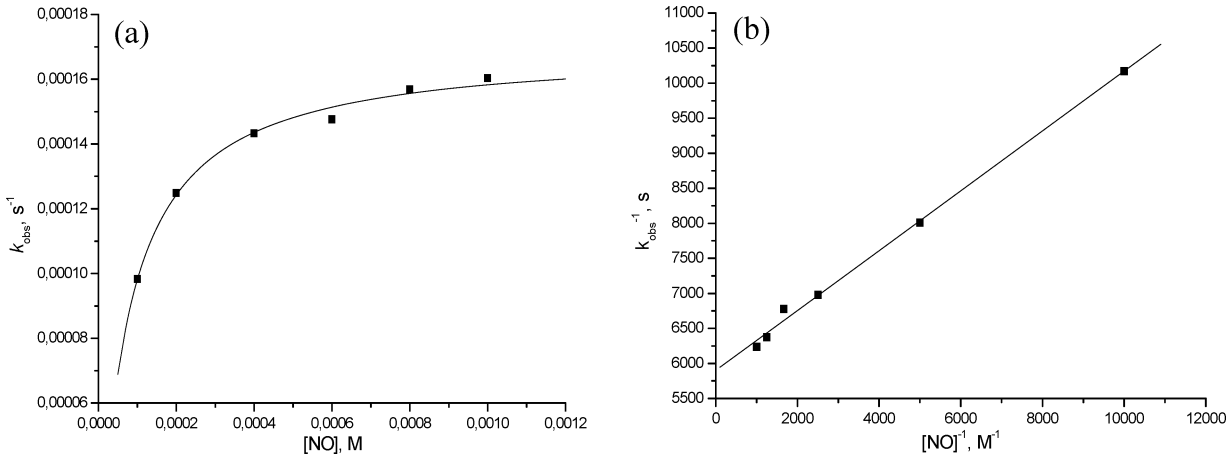

Figure 12. (a) Plot of k_{obs} versus [NO] for the reductive nitrosylation of $(P^{16-})Fe^{II}(H_2O)(NO^+)$. (b) Plot of k_{obs}^{-1} versus $[NO]^{-1}$. Experimental conditions: $[(P^{16-})Fe^{III}] = 2.0 \times 10^{-5}$ M, pH 6.5 (0.05 M Mes), temp. = 25 °C, $\lambda_{det} = 431$ nm, $I = 0.1$ M $NaClO_4$.

Table 9. Rate and Activation Parameters for Nitrite-Induced Reductive Nitrosylation of $(P^n)Fe^{II}(H_2O)(NO^+)$ and $(P^n)Fe^{II}(OH)(NO^+)$ at 25 °C

iron(III) porphyrin	pK_a	pH	k_{red}[a] (s^{-1})	slope[b] ($M^{-1}\,s^{-1}$)	k_{nit} ($M^{-1}\,s^{-1}$)	$\Delta H^{\ddagger}$ (kJ mol^{-1})	$\Delta S^{\ddagger}$ (J $mol^{-1}\,K^{-1}$)	$\Delta V^{\ddagger}$ ($cm^3\,mol^{-1}$)
$(P^{16-})Fe$[c]	9.9	6.5	$(1.7 \pm 0.2) \times 10^{-4}$	$(1.3 \pm 0.2) \times 10^{-2}$	$(1.4 \pm 0.2) \times 10^{-2}$	80 ± 1	-11 ± 3	-9.8 ± 0.4
$(P^{8-})Fe$[d]	9.3	7	$(2.8 \pm 0.2) \times 10^{-4}$	1.6 ± 0.1	2.1 ± 0.2	60 ± 2	-36 ± 7	-8.6 ± 0.4
$(TPPS^{4-})Fe$[e]	7.0	5	$(4.6 \pm 0.4) \times 10^{-4}$	2.2 ± 0.1	3.1			
$(TMPyP^{4+})Fe$[f]	5.5	4.5	7×10^{-3} [g]	15.0 ± 0.1	42 ± 3	88 ± 2	$+92 \pm 6$	$+8.8 \pm 0.1$
$(P^{8+})Fe$[d]	5.0	2	$(4.0 \pm 0.2) \times 10^{-2}$	55 ± 3	155 ± 5	90 ± 3	$+99 \pm 10$	$+7.2 \pm 0.5$
		4		89 ± 1	242 ± 7	73 ± 2	$+92 \pm 7$	$+12.3 \pm 0.7$

[a] Calculated values using eq 12 when no nitrite was added. [b] Value calculated from k_{obs} versus $[NO_2^-]$ at constant [NO]. [c] This work. [d] Ref 18. [e] Measured at 15 °C, ref 17. [f] Ref 6a. [g] Observed rate constant (k_{obs}) for the studied reaction.

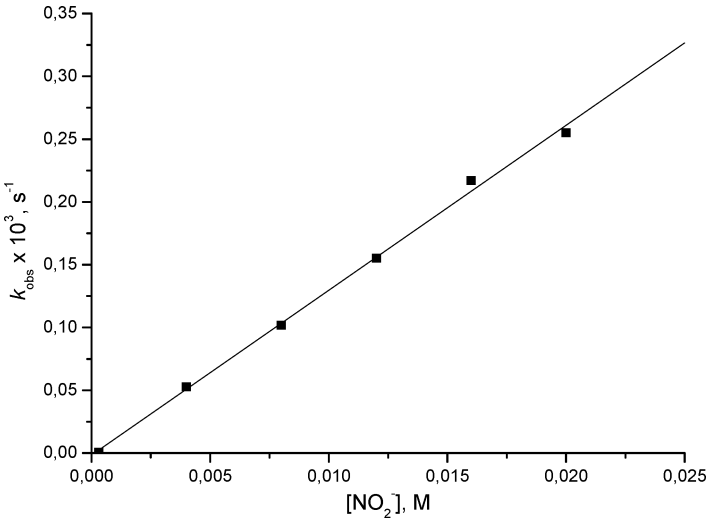

Figure 13. Nitrite concentration dependence of the reductive nitrosylation of $(P^{16-})Fe^{II}(H_2O)(NO^+)$. Experimental conditions: $[(P^{16-})Fe^{III}] = 3.0 \times 10^{-5}$ M, [NO] = 1 mM, temp. = 25 °C, λ_{det} = 431 nm, pH 6.5 (0.05M Mes), I = 0.1 M (with $NaClO_4$).

excellently to the linear free-energy relationship (LFER) reported for the nucleophilic addition (OH^-) rate constant and the redox potential for a series of *trans*-tetrapyridine ruthenium nitrosyl complexes.[32] For the $k_{OH} = 1.0 \times 10^3$ $M^{-1}\,s^{-1}$ value found for the present complex, the reported correlation predicts a redox potential of 0.21 V, which is in perfect agreement with our experimental value. According to the data referenced, the ruthenium complexes have lower rate constants because of the steric hindrance of pyridine ligands which are free to rotate. In the present case, the malonate substituents on the porphyrin cause sufficient steric hindrance such that the $(P^{16-})Fe^{II}(H_2O)(NO^+)$ complex also fits the reported LFER.

Suggested Mechanisms and Comparison with Other Iron(III) Porphyrins. A. Reactivity of $(P^{16-})Fe^{III}(H_2O)_2$ and $(P^{16-})Fe^{III}(OH)$ toward NO. Mechanistic information on the *on* and *off* reactions of NO with $(P^{16-})Fe^{III}(H_2O)_2$ can best be obtained from the volume profile presented in Figure 5. The positive activation volumes for the binding and release of NO favor a dissociative mechanism which is analogous to that reported for a series of diaqua-ligated porphyrins summarized in Table 4. The overall volume change observed for the reaction is not only the result of the displacement of water by NO but also of a change in spin state from S = 3/2, 5/2 for the diaqua complex to $S = 0$ for the Fe^{II} nitrosyl complex. The data in Table 4 show that the rates for NO binding correlate to some extent with the contribution of the intermediate spin state (Int %) in the spin-admixed state (S = 3/2, 5/2). As mentioned above, increasing Int % correlates with increasing lability of the ligand on the metal center as influenced by the increasing electron-donating properties of the meso substituents on the porphyrin. The trend in $\Delta V^{\ddagger}_{on}$ along the series of complexes suggests a gradual changeover from a dissociative mechanism for the anionic complexes to a dissociative interchange mechanism for the cationic complexes. Almost similar trends are observed for the water exchange reactions for the series of $(P)Fe^{III}(H_2O)_2$ complexes summarized in Table 4. The magnitude of the water exchange rate constant and the close agreement between the volumes of activation for the water exchange process and the binding of NO, suggest that the rate and mechanism of the latter process is controlled by the water exchange process of the diaqua complexes.[4,5,7c,33] Thus, electron-donating substituents on the porphyrin induce a dissociative mechanism by weakening the $Fe-OH_2$, whereas electron-withdrawing substituents strengthen the $Fe-OH_2$ bond and tend to favor a dissociative interchange mechanism.

The rate constants for the dissociation of NO from the nitrosyl complex $(P)Fe^{II}(H_2O)(NO^+)$ summarized in Table 4 show for some of the complexes the trend that the nitrosyl complex is stabilized by positively charged as compared to

(32) (a) Videla, M.; Jacinto, J. S.; Baggio, R.; Garland, M. T.; Singh, P.; Kaim, W.; Slep, L. D.; Olabe, J. A. *Inorg. Chem.* **2006**, *45*, 8608 (b) Roncaroli, F.; Ruggiero, M. E.; Franco, D. W.; Estiu, G. L. Olabe, J. A. *Inorg. Chem.* **2002**, *41*, 5760

(33) (a) Helm, L.; Merbach, A. E. *Chem. Rev.* **2005**, *105*, 1923. (b) Richens, D. T. *Chem. Rev.* **2005**, *105*, 1961.

negatively charged substituents on the porphyrin. This observation is in agreement with results from Raman resonance and DFT studies.[34] In general, the value of $\Delta V^{\ddagger}_{off}$ is more positive than of $\Delta V^{\ddagger}_{on}$ since the *off* reaction involves bond cleavage, formal oxidation of Fe^{II} to Fe^{III}, accompanied by a spin-state change ($S = 0$ to $S = 3/2$, 5/2), and solvent reorganization resulting from the charge neutralization during $Fe^{II}-NO^+$ bond cleavage.[3]

The reversible binding of NO at higher pH revealed a different kinetic behavior for the monohydroxo-ligated $(P^{16-})Fe^{III}(OH)$ complex compared to that of the (P^{16-})-$Fe^{III}(H_2O)_2$ complex, as indicated by the negative activation parameters, namely, $\Delta S^{\ddagger}_{on} = -82 \pm 4$ J mol^{-1} K^{-1} and $\Delta V^{\ddagger}_{on} = -9.4 \pm 0.2$ cm^3 mol^{-1}. It was in general concluded that the slow rate constant for NO binding to complexes of the type $(P)Fe^{III}(OH)$ is mainly controlled by the $Fe^{II}-NO^+$ bond-formation step and the accompanying electronic and structural changes, rather than the lability of the metal center.[4,5] Electronic changes for the formation of the $Fe^{II}-NO^+$ bond are accompanied by reorganization of the spin arrangement in the iron(III) center from high spin ($S = 5/2$) to low spin (diamagnetic, $S = 0$). In addition, structural changes as a result of the iron center that moves from out-of-plane to in-plane during bond formation are also expected.[5b] These conclusions suggest that the larger spin and structural changes for the monohydroxo-ligated species $(P)Fe^{III}(OH)$ demand a higher activation barrier for NO binding and release, such that lower reaction rates were observed. The observed results are consistent with the earlier findings for related complexes summarized in Table 6.[5] The rate-determining step for NO binding to $(P^{16-})Fe^{III}(OH)$ via an associative addition mechanism is mainly controlled by electronic changes on the Fe^{III} center and the accompanying structural rearrangement. Larger spin and structural changes during the formation and breakage of the $Fe^{II}-NO^+$ bond accompanied by higher activation barriers account for the slower reactions in the case of the monohydroxo ligated species (see rate data in Table 6).

We propose in the mechanistic scheme outlined in reaction 16 that NO binding to five-coordinate $(P^{16-})Fe^{III}(OH)$ involves the formation of a diffusion-controlled encounter complex $\{(P^{16-})Fe^{III}(OH) \,||\, NO\}$, followed by the activation step for the formation of the $Fe^{II}-NO^+$ bond, similar to that suggested for high-spin 5-coordinate monohydroxo ligated iron(III) porphyrins.[35]

$$(P^{16-})Fe^{III}(OH) + NO \underset{K_{-D}}{\overset{k_D}{\rightleftharpoons}} \{(P^{16-})Fe^{III}(OH) \,||\, NO\} \xrightarrow{k} [(P^{16-})Fe^{III}(OH)\cdots NO]^{\ddagger} \rightarrow (P^{16-})Fe^{II}(OH)(NO^+) \quad (17)$$

On the basis of the results summarized in Tables 4 and 6, $(P)Fe^{III}(OH)$ complexes follow an associatively activated addition mechanism for NO binding and show slower binding rates in contrast to a dissociatively activated mode observed for $(P)Fe^{III}(OH_2)_2$ complexes. Furthermore, the reported values for k_{on} vary by a factor of approximately 10^2 for the diaqua-ligated porphyrins and appear to correlate with the contribution of the intermediate spin state, $S = 3/2$. In comparison, however, differences in the NO binding rate constants are rather small for all studied $(P)Fe^{III}(OH)$ complexes. This difference is because the lability of the Fe^{III} complex controls the rate of NO binding to the six-coordinate $(P)Fe^{III}(OH_2)_2$ complexes, which does not play a role in the case of the five-coordinate $(P)Fe^{III}(OH)$ complexes.

The volume profile for the binding of NO to $(P^{16-})Fe^{III}(OH)$ is shown in Figure 8, from which it can clearly be seen that the overall reaction volume ($\Delta V = \Delta V^{\ddagger}_{on} - \Delta V^{\ddagger}_{off}$) has a value of -24.4 ± 0.6 cm^3 mol^{-1}, which is close to a value of approximately -23 cm^3 mol^{-1} found for several other hydroxo complexes (except for $(P^{8+})Fe^{III}$, see data in Table 6). This large overall volume collapse for the binding of NO is partially caused by the formation of the Fe−NO bond and the change in spin state from a five-coordinate high-spin hydroxo reactant to a six-coordinate, diamagnetic (low-spin) nitrosyl product. The activation volumes reported for $(P^{16-})Fe^{III}(OH)$ and $(P^{8-})Fe^{III}(OH)$ suggest an "early" transition state for the *on* reaction and a "late" transition state for the *off* reaction, compared to the opposite trend for the other complexes cited in Table 6. This is also in the value of K_{NO} in terms of the more effective binding of NO.

From the data summarized in Table 7, it is clearly seen how the rate constants for the binding and release of NO decrease on going from $(P)Fe^{III}(OH_2)_2$ to $(P)Fe^{III}(OH)$ for the series of complexes. This is throughout ascribed to the role of the electronic barriers involved in the reactions with the $(P)Fe^{III}(OH)$ complexes. These different decreases arise from the characteristic electronic and structural properties among the complexes studied $(P)Fe^{III}(OH_2)_2$. In purely high-spin five-coordinate $(P)Fe^{III}(OH)$ complexes, it normally demands larger reorganization of the spin state of the metal center and structural changes with rather small variation in k_{on}^{OH} for the studied complexes. While larger ratios for the NO binding rate constants ($k_{on}^{H_2O}/k_{on}^{OH}$) are observed for $(P^{n-})Fe^{III}$ complexes, resulting from mainly high k_{on} values, smaller ratios are observed for the $(P^{n+})Fe^{III}$ complexes.

B. Subsequent Reductive Nitrosylation of $(P^{16-})Fe^{II}(H_2O)(NO^+)$. Our report[18] on the reactivity of ferric nitrosyl complexes as a function of the nature of the porphyrin substituents, indicates that kinetic and mechanistic features of the subsequent reductive nitrosylation reaction of negatively charged porphyrins, $(P^{n-})Fe^{II}(H_2O)(NO^+)$, differs from that found for positively charged porphyrins, $(P^{n+})Fe^{II}(H_2O)$-(NO^+). The observed reduction of coordinated NO^+ is catalyzed by the addition of nitrite to the reaction solution. It was further concluded that the rate of nitrite-catalyzed reduction of $(P)Fe^{II}(H_2O)(NO^+)$ depends on the electrophilicity of coordinated NO^+ and the nature of the reactant, namely, NO_2^- or HONO. The available results (see Table 9) favor the operation of an inner-sphere electron-transfer process between nitrite and coordinated NO^+. Charge

(34) (a) Linder, D. P.; Rodgers, K. P.; Banister, J.; Wyllie, G. R. A.; Ellison, M. K.; Scheidt, W. R. *J. Am. Chem. Soc.* **2004**, *126*, 14136. (b) Linder, D. P.; Rodgers, K. R. *J. Am. Chem. Soc.* **2005**, *44*, 1367.
(35) (a) Franke, A.; Stochel, G.; Jung, Ch.; van Eldik, R. *J. Am. Chem. Soc.* **2004**, *126*, 4181. (b) Laverman, L. E.; Ford, P. C. *J. Am. Chem. Soc.* **2001**, *123*, 11614 and references therein.
(36) Gruhn, N. E.; Lichtenberger, D. L.; Ogura, H.; Walker, F. A. *Inorg. Chem.* **1999**, *38*, 4023.

neutralization during bond formation between NO_2^- and NO^+ on positively charged $(P^{n+})Fe^{II}(H_2O)(NO^+)$ complexes largely accounts for the positive activation entropies and volumes associated with this process. In contrast, negative values for these activation parameters observed for the reaction with the negatively charged $(P^{n-})Fe^{II}(H_2O)(NO^+)$ complexes suggest that bond-formation and charge concentration account for the observed data. These conclusions are in good agreement with the experimental data found for the nitrite-induced reductive nitrosylation of $(P^{16-})Fe^{II}(H_2O)(NO^+)$ as shown in Table 9. The rate of NO_2^- coordination (k_{nit}) to the nitrosyl complex is faster for $(P^{n+})Fe^{II}(H_2O)(NO^+)$ than that for $(P^{n-})Fe^{II}(H_2O)(NO^+)$. For example, the observed rate constants for the binding of NO_2^- to $(P^{16-})Fe^{II}(H_2O)(NO^+)$ decrease by a factor of 10^4 compared to that observed for $(P^{8+})Fe^{II}(H_2O)(NO^+)$ and are even 10^2 times slower than those for $(P^{8-})Fe^{II}(H_2O)(NO^+)$. This again indicates that the crucial factor that controls the rate of reductive nitrosylation is the overall negative charge on the porphyrin that increases the electron density on metal center and reduces the electrophilicity of coordinated NO^+. Thus direct nucleophilic attack of nitrite on coordinated NO^+ is suggested as rate-determining step to form a $(P)Fe^{II}-N_2O_3$ intermediate that subsequently releases N_2O_3 and rapidly reacts with NO to form $(P)Fe^{II}-NO$. From the data in Table 9, an increase in activation volume for nitrite binding to $(P)Fe^{II}(H_2O)(NO^+)$ on going from $(P^{16-})Fe^{III}$ to $(P^{8+})Fe^{III}$ clearly shows that the contribution of bond formation is facilitated by negatively charged meso substituents, while a decreasing electrostriction prevails over bond-formation in porphyrins containing electron-donating substituents.

Conclusions

The presented results provide mechanistic information on the reaction of NO with an extremely negatively charged porphyrin complex, $(P^{16-})Fe^{III}$. The speciation of $(P^{16-})Fe^{III}$ in aqueous solution depends on pH and involves the formation of diaqua- and monohydroxo-ligated complexes. The experimental data obtained for $(P^{16-})Fe^{III}(H_2O)_2$ in comparison with the reported reactivity pattern for other water-soluble $(P)Fe^{III}(H_2O)_2$ porphyrins demonstrate that the number and nature of charged substituents on the porphyrin affect the dynamics of the water exchange reaction and the reversible binding of NO, in which both processes follow a dissociative substitution mechanism. For the five-coordinate $(P^{16-})Fe^{III}(OH)$ complex, the addition of NO follows an associative bond formation process which is in agreement with that found for a series of $(P)Fe^{III}(OH)$ porphyrins. The nitrosyl adduct $(P^{16-})Fe^{II}(H_2O)(NO^+)$ is subjected to slow reductive nitrosylation that is catalyzed by nitrite to yield $(P^{16-})Fe^{II}(NO)$ as product via an inner-sphere redox pathway. The rate-limiting step of this process shows that the reaction is controlled by the electrophilicity of coordinated NO^+. Importantly, the potential catalytic activity of hydroxide ions during reductive nitrosylation was found to be several orders of magnitude larger than for the nitrite-catalyzed process.

Acknowledgment. The authors gratefully acknowledge financial support from the Deutsche Forschungsgemeinschaft as part of SFB 583 on Redox-Active Metal Complexes and the European Commission within AQUACHEM Research Training Network Contract MRTN-CT-2003-503864.

Supporting Information Available: Figures S1−S7 that present the ^{17}O NMR measurement and temperature and pressure dependencies of the individual reactions studied and Figure S8 showing the hydroxide concentration dependence of the reductive nitrosylation reaction of $(P^{16-})Fe^{II}(H_2O)(NO^+)$. This material is available free of charge via the Internet at http://pubs.acs.org.

IC061732G